JOURNAL OF MOLECULAR SPECTROSCOPY **146,** 8–48 (1991)

The Use of Extended Permutation-Inversion Groups in Constructing Hyperfine Hamiltonians for Symmetric-Top Internal Rotor Molecules like $H_3C–SiH_3$

JON T. HOUGEN

Molecular Physics Division, National Institute of Standards and Technology, Gaithersburg, Maryland 20899

W. LEO MEERTS

Fysisch Laboratorium, University of Nijmegen, Toernooiveld, 6525 ED Nijmegen, The Netherlands

AND

IRVING OZIER

Department of Physics, University of British Columbia, 6224 Agriculture Road, Vancouver, Canada V6T 2A6

The m-fold extended group $G_{18}^{(m)}$, corresponding to the permutation-inversion group G_{18} for molecules like $H_3C–SiH_3$, has been obtained. In this group, m is the smallest integer for which $m\rho$ is also an "integer," where ρ is the usual ratio of the moment of inertia of the top about the A axis to the moment of inertia of the molecule about the A axis. The extended group has $18m$ elements, divided into $(9m+3)/2$ or $(9m+6)/2$ classes, for odd and even values of m, respectively. Using this group, it is possible to assign definite symmetry species in an internal-axis-method (IAM) treatment to laboratory-fixed, molecule-fixed, top-fixed, and frame-fixed projections of various vector operators, thus making it possible to express the spin–rotation and spin–spin contributions to the hyperfine interaction operator in terms of rotational angular momentum components, nuclear-spin angular momentum components, and functions of the torsional angle, all of which have known symmetry species and selection rules in the IAM basis set. Using a hyperfine Hamiltonian constructed on the basis of these considerations, together with a recent treatment of the two-level problem modified to take into account large first-order Stark effects, it is possible to rationalize the pattern of observed and unobserved avoided-crossing signals in recent molecular beam studies of symmetric-top internal rotor molecules. With this understanding, it also proved possible to detect for the first time one of the "missing" avoided-crossing signals in CH_3SiH_3.

1. INTRODUCTION

In a series of earlier papers (*1–8*), two of the authors have developed and applied a new avoided-crossing molecular beam electric resonance technique for directly determining: (i) the A (or C) rotational constant of symmetric-top molecules, (ii) the torsional splittings (and thus the barrier heights) for symmetric-top molecules exhibiting high-barrier internal rotation motion, and (iii) a variety of other parameters associated with symmetry axis rotation and internal rotation motions in symmetric-top molecules.

0022-2852/91 $3.00

This technique requires the existence of a Stark-tuned avoided crossing. Two levels that could be brought by an external Stark field into exact energy coincidence, if there were no connecting matrix element, repel each other and do not cross. It was established (*1–8*) that, depending on the quantum numbers involved, the necessary coupling could be produced by the rotationally generated dipole moment perpendicular to the symmetry axis (*9*), or by the nuclear hyperfine interactions.

However, a troubling puzzle remained. It was found for CH_3SiH_3 (*5*), CH_3SiF_3 (*6*), and CH_3CD_3 (*7*) that certain avoided crossings could not be observed, in spite of their apparent similarity to those which were easily detected. For reasons inherent in the standard two-level problem (*10*), a small magnitude for the coupling matrix element was not considered to be an adequate explanation for the anomaly: Within the framework of the standard two-level problem, the transition probability can in principle always be made unity by increasing the strength of the driving field, provided only that the coupling matrix element is nonzero. It was tentatively concluded (*5, 6*) that the matrix elements involved must vanish, but further investigation (*7*) showed that in fact the necessary coupling could be provided by the spin–spin interaction between nuclei in the top and frame rotors of these molecules. This puzzle provided the initial motivation for the current work.

The present paper has evolved to serve three purposes. First, the extended group (*11*) introduced for the asymmetric rotor F_3C–NO (*12*) is applied for the first time to the torsion–rotation problem in a symmetric top. This may facilitate analysis of high-precision data on torsion–rotation–vibration energy levels (*13, 14*). Second, the extended group is used to develop the nuclear hyperfine Hamiltonian in molecules such as H_3C–SiH_3. This lays the ground work for analysis of the nuclear hyperfine splittings that can now be observed by molecular beam techniques. Finally, a formalism is developed to evaluate mixing matrix elements arising from the spin–spin interaction. In an attempt to use these matrix elements properly, we have recently considered the two-level problem for a symmetric top where at least one level has a linear Stark effect (*15*) and found that the transition probability cannot always be made unity. In fact, if the transition moment is small enough, the transition will be unobservable. The mixing matrix elements evaluated here are thus used in conjunction with these modified two-level transition probabilities (*15*) to explain the avoided-crossing anomalies (*5–7*) that formed the initial puzzle.

For a symmetric rotor, both the principal-axis method (PAM) and the internal-axis method can easily be used to diagonalize the torsional Hamiltonian (*16*), and hence to treat vibronic, rotational, and nuclear spin problems. While the PAM is inherently simpler, it has the serious disadvantage that, in the high barrier limit, the problem does not readily reduce to that of a rigid rotor and a small-amplitude torsional oscillator (*16*). Thus, for example, it is difficult to isolate nuclear hyperfine terms which vanish in the high-barrier limit from those which would be present in simpler systems such as CH_3F. On the other hand, the IAM does separate such terms "properly," an advantage which is particularly important in the early stages of an analysis. Unfortunately, in the IAM, the torsional and rotational wavefunctions, as well as many operators, do not transform properly according to the irreducible representations of the G_{18} permutation-inversion group (*17*), and the derivation of selection rules cannot be carried out in the IAM by conventional group-theoretical methods. It is in

large part to overcome this last difficulty that the extended-group formalism has been introduced.

The extended-group formalism (*11*) developed here for molecules like H_3C–SiH_3 is based on many of the ideas used in an earlier extended-group treatment (*12*) for molecules like F_3C–NO. The reasoning leading to the introduction of the extended group can be described for the F_3C–NO case as follows. One begins with the Longuet-Higgins permutation-inversion group (*17*) for F_3C–NO, which contains as one of its elements the cyclic permutation (123), if the three fluorines are numbered 1, 2, and 3, respectively. In this permutation-inversion group, $(123)^3$ is clearly equivalent to the identity operation, since the net result of three successive (123) interchanges is that no fluorines have been interchanged. However, in an IAM treatment (*16*) of F_3C–NO, each forward rotation of the CF_3 top is accompanied by a smaller backward rotation of the whole molecule (to cancel any angular momentum generated by the internal rotation motion). Thus, since $(123)^3$ represents a 2π rotation of the CF_3 top in, say, the forward direction, it must be accompanied in the IAM treatment by some rotation less than 2π of the whole molecule in the backward direction. Since the molecule is not restored to its original position in space by these two rotations, the operation $(123)^3$ does not correspond exactly to the identity operation. If, however, we now perform $(123)^3$ m times, i.e., if we perform $(123)^{3m}$, then for a suitably chosen (and perhaps large) integer m, the molecule can be returned arbitrarily close to its original position. It is the existence of the extra operations $(123)^n$ with $4 \leqq n \leqq 3m - 1$ which gives rise to the additional elements in the extended group. The reader is referred to Ref. (*12*) for a description of the mathematics corresponding to the words in this paragraph.

On another historical note, one of the authors proposed some time ago (*18*) the use of a *double* group for molecules like H_3C–SiH_3. This value of $m = 2$ for the extended group arose because the coordinate system considered in (*18*) for H_3C–SiH_3 was closely analogous to the IAM coordinate system appropriate for molecules like H_3C–CH_3, with two identical coaxial rotors. However, for molecules like H_3C–SiH_3, with two nonidentical rotors, the coordinate system of (*18*) has neither the high-barrier advantages of the IAM system (*16*) nor the simplicity of the principal-axis-method system (*16*). It is our present opinion that the approach taken in (*18*), while not technically wrong, is nevertheless ill-advised. Values of $m \neq 2$, as determined in the present paper, are clearly to be preferred.

The remainder of this paper is divided into three main parts. In Section 2, the coordinate system, symmetry operations, and group theory are dealt with. In Section 3, the spin–rotation and spin–spin contributions to the hyperfine Hamiltonian are explicitly constructed, in terms of operators having known symmetry properties and selection rules. In Section 4, the application to the anticrossing anomalies is discussed.

2. EXTENDED-GROUP THEORY

A. IAM Coordinate System

We here follow closely the procedures of (*12*), expressing the Cartesian coordinates of the atoms in terms of the vibrational and rotational variables used in the molecular wavefunction through the equation

$$\mathbf{R}_i = \mathbf{R} + S^{-1}(\chi\theta\phi)[\mathbf{a}_i(\alpha) + \mathbf{d}_i], \tag{1}$$

where the 3×1 column matrices $\mathbf{R}_i$ and $\mathbf{R}$ contain the laboratory-fixed components of the position vector of atom i and of the molecular center of mass, respectively; the 3×3 matrix $S^{-1}(\chi\theta\phi)$ contains the direction cosines, defined for $S^{+1}(\chi\theta\phi)$ in Eq. (4) of (*12*) as functions of the rotational (Eulerian) angles; the 3×1 column matrix $\mathbf{a}_i(\alpha)$ contains the molecule-fixed components of the reference configuration obtained after an internal rotation through the torsional angle α (to be defined more completely below); and the 3×1 column matrices $\mathbf{d}_i$ contain the molecule-fixed components of the infinitesimal displacement vectors used to describe the small-amplitude vibrational degrees of freedom.

Before defining the reference configuration, it is convenient to imagine a molecule like $H_3C\text{–}SiH_3$ as consisting of a coaxial top rotor (e.g., the CH_3 group) and frame rotor (e.g., the SiH_3 group). The atom numbering scheme adopted here is illustrated in Fig. 1, indicating that hydrogens 1, 2, 3 are in the top, while hydrogens 4, 5, 6 are in the frame. It is then convenient to define the reference configuration $\mathbf{a}_i(\alpha)$ in terms of an initial configuration $\mathbf{a}_i^0$ through the equations

$$\begin{aligned} \mathbf{a}_i(\alpha) &\equiv S_i^{-1}(\alpha, 0, 0) \cdot \mathbf{a}_i^0 \\ S_i^{-1}(\alpha, 0, 0) &\equiv S^{-1}(-\alpha\rho + \alpha, 0, 0), \qquad i \subset \text{top} \\ S_i^{-1}(\alpha, 0, 0) &\equiv S^{-1}(-\alpha\rho, 0, 0), \qquad i \subset \text{frame}, \end{aligned} \tag{2}$$

where

$$\rho \equiv I_{\text{top}}/(I_{\text{top}} + I_{\text{frame}}) \tag{3}$$

is the usual ratio (*16*) of moments of inertia about the internal rotation axis occurring in symmetric-top problems. The quantity $+\alpha$ occurring in the argument of S^{-1} for

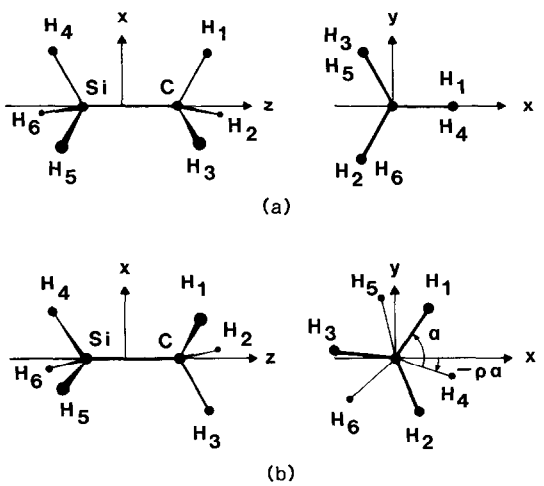

FIG. 1. (a) The initial configuration $\mathbf{a}_i^0$ as defined in Table I. For the initial configuration, the xz plane is a plane of symmetry. (b) An internally rotated reference configuration $\mathbf{a}_i(\alpha)$, as defined by Eqs. (2), for $\alpha \cong +75°$ and $\rho \cong \frac{1}{4}$.

TABLE I

The Initial Configuration[a] $\mathbf{a}_i^0$ for Use in Eqs. (2)

Atom	$(a_i^o)_x$	$(a_i^o)_y$	$(a_i^o)_z$	Atom	$(a_i^o)_x$	$(a_i^o)_y$	$(a_i^o)_z$
H_1	$(a_t^o)_x$	0	$(a_t^o)_z - A_z$	H_4	$(a_f^o)_x$	0	$(a_f^o)_z - A_z$
H_2	$(-1/2)(a_t^o)_x$	$(-\sqrt{3}/2)(a_t^o)_x$	$(a_t^o)_z - A_z$	H_5	$(-1/2)(a_f^o)_x$	$(+\sqrt{3}/2)(a_f^o)_x$	$(a_f^o)_z - A_z$
H_3	$(-1/2)(a_t^o)_x$	$(+\sqrt{3}/2)(a_t^o)_x$	$(a_t^o)_z - A_z$	H_6	$(-1/2)(a_f^o)_x$	$(-\sqrt{3}/2)(a_f^o)_x$	$(a_f^o)_z - A_z$
C	0	0	$(a_C^o)_z - A_z$	Si	0	0	$(a_{Si}^o)_z - A_z$

$A_z = [3m_H(a_t^o)_z + 3m_H(a_f^o)_z + m_C(a_C^o)_z + m_{Si}(a_{Si}^o)_z]/(3m_H + 3m_H + m_C + m_{Si})$

[a] CH bond lengths for the top are given by $\{(a_t^o)_x^2 + [(a_t^o)_z-(a_C^o)_z]^2\}^{1/2}$; SiH bond lengths for the frame are given by $\{(a_f^o)_x^2 + [(a_f^o)_z-(a_{Si}^o)_z]^2\}^{1/2}$. The quantity A_z insures that the center of mass of the initial configuration lies at the origin.

top atoms gives rise to the internal rotation of the top with respect to the frame; the quantity $-\alpha\rho$ in the argument for both top and frame atoms gives rise to the backward rotation of the whole molecule. Atom positions $\mathbf{a}_i^0$ in the initial configuration, which are taken to be constants (and thus unaffected by differentiation, symmetry operations, etc.), are given in Table I in terms of the various bond lengths in the molecule.

Constraint equations for the small-amplitude displacement vectors $\mathbf{d}_i$ are as given in Eq. (14) of (*12*). Since the $\mathbf{d}_i$ will be neglected in this paper, these constraints will not be discussed further. Again as in (*12*), the reference configuration itself satisfies a number of equations:

$$\sum_i m_i \mathbf{a}_i(\alpha) = \mathbf{0}$$

$$\sum_i m_i \mathbf{a}_i(\alpha) \cdot (d\mathbf{a}_i/d\alpha) = 0$$

$$\sum_i m_i \mathbf{a}_i(\alpha) \times (d\mathbf{a}_i/d\alpha) = \mathbf{0}. \tag{4}$$

The first of these indicates that the center of mass of the reference configuration remains at the origin during internal rotation. The second holds because bond lengths are not permitted to vary during internal rotation in the model adopted. The third equation indicates that no angular momentum is generated during the internal rotation motion; i.e., the coordinate system used for the reference configuration is an IAM coordinate system (*16*). It is the third equation which leads to the value of ρ given in Eq. (3).

B. Symmetry Operations and Group Generators

The point group appropriate for a molecule like H_3C–SiH_3 in either a staggered or an eclipsed equilibrium geometry is C_{3v}. The permutation-inversion group G_{18} appropriate for molecules like H_3C–SiH_3 when internal rotation motion occurs has been

given by Bunker (*19*). His character table for this group is reproduced in Table II. It can be seen that the group has two nondegenerate representations, A_1 and A_2, and four doubly degenerate representations E_1, E_2, E_3, and E_4. For the atom labeling of Fig. 1, the latter correspond to functions which are invariant to: rotation of the top alone, rotation of the frame alone, internal rotation of the molecule, and rotation of the whole molecule, respectively. (Although the handedness of the atom labeling scheme adopted here differs from that in Ref. (*19*), this difference affects neither the correspondence above nor the character table.)

If the effect of the cyclic permutation (123) on a function of the laboratory-fixed Cartesian coordinates $\mathbf{R}_i$ is defined to be

$$(123)\cdot f(\mathbf{R}_1, \mathbf{R}_2, \mathbf{R}_3, \mathbf{R}_C, \mathbf{R}_4, \mathbf{R}_5, \mathbf{R}_6, \mathbf{R}_{Si}) \equiv +f(\mathbf{R}_2, \mathbf{R}_3, \mathbf{R}_1, \mathbf{R}_C, \mathbf{R}_4, \mathbf{R}_5, \mathbf{R}_6, \mathbf{R}_{Si}), \quad (5)$$

etc., then it can be shown by direct substitution in Eqs. (1) and (2) that the variable transformations given in Table III are equivalent to the permutation-inversion operations indicated. From the second line in Table III, we see that the operation $(123)^3$ does not represent the identity when applied to the rotational part of the molecular wavefunction, though it must of course be the identity when applied to the full wavefunction. It is this peculiar behavior of $(123)^3$ which leads to the introduction of an extended group (*12*).

Let us now define three generators for the extended group,

$$C_t \equiv (123)$$
$$C_f \equiv (456)$$
$$\sigma \equiv (23)(56)^*, \quad (6)$$

TABLE II

Character Table for the Permutation-Inversion Group G_{18} for H_3C–SiH_3[a]

[n][b] PI[c]	[1] E	[2] (123)	[2] (456)	[2] (123)(456)	[2] (123)(465)	[9] (23)(56)*
A_1	1	1	1	1	1	1
A_2	1	1	1	1	1	-1
E_1	2	2	-1	-1	-1	0
E_2	2	-1	2	-1	-1	0
E_3	2	-1	-1	2	-1	0
E_4	2	-1	-1	-1	2	0

[a] From Ref. (19).
[b] Number of permutation-inversion operations in each class. When the number is 2, the class consists of an element and its inverse.
[c] A representative permutation-inversion element from each class, described using the atom numbering scheme of Fig. 1. (The slight difference in numbering from that used in Ref. (19) does not change the form of the character table from that given in Ref. (19).)

TABLE III

Transformations of the Variables on the Right Side of Eq. (1) Corresponding to Various Permutation-Inversion Operations[a] on the Left Side of Eq. (1)

PI[a]	GEN[b]	c-o-m[c]	ROTN[d]	INT ROTN[d]	VIBRATION[e]	j = fcn(i)[e]
E		R	χ,θ,ϕ	α	$\mathbf{d}_i$	
(123)	C_t	+R	$\chi-2\pi\rho/3,\theta,\phi$	$\alpha-2\pi/3$	$C_{3/\rho}^{-1}\mathbf{d}_j$	$j = i$, $i \subset$ frame; $\mathbf{a}_j^o = C_3^{+1}\mathbf{a}_i^o$, $i \subset$ top
(456)	C_f	+R	$\chi-2\pi(\rho-1)/3,\theta,\phi$	$\alpha-2\pi/3$	$C_{3/(\rho-1)}^{-1}\mathbf{d}_j$	$j = i$, $i \subset$ top; $\mathbf{a}_j^o = C_3^{-1}\mathbf{a}_i^o$, $i \subset$ frame
(23)(56)*	σ	-R	$\pi-\chi,\pi-\theta,\pi+\phi$	$-\alpha$	$\sigma_v\mathbf{d}_j$	$\mathbf{a}_j^o = \sigma_v^{-1}\mathbf{a}_i^o$

[a]The permutation-inversion operations act on the laboratory-fixed components of the position vectors of each atom $\mathbf{R}_i$, using the numbering scheme of Fig. 1.
[b]The symbols for the generators of the extended group of G_{18} are to be used in Eqs. (7-9).
[c]Laboratory-fixed components of the position vector of the center-of-mass.
[d]The rotational (Eulerian) angles and the internal rotation angle.
[e]Infinitesimal displacement vectors for the small amplitude vibrations. The subscript j is defined as a function of the subscript i by the relations between initial vectors $\mathbf{a}_i^o$ indicated in the last column of the table, where $C_s^{\pm 1}$ corresponds to $S^{\pm 1}(2\pi/s,0,0)$ with $s = 3$, $3/\rho$ or $3/(\rho-1)$, and where the rotation matrix S^{+1} is given in Eq. (4) of Ref. (12); $\sigma_v = \sigma(xz)$.

where the equalities in Eqs. (6) are meant to indicate that these generating operations have the effects on the vibration–rotation variables in the molecular wavefunction indicated in the corresponding rows of Table III. If, following (*12*), we now chose the lowest integer m such that $m\rho$ is also an integer p to within the desired precision (e.g., to within the experimental error on ρ), then it can be seen that the generating equations obeyed by the operations in Eqs. (6) become

$$C_t^{3m} = C_f^{3m} = \sigma^2 = E, \qquad C_t\sigma = \sigma C_t^{3m-1}$$

$$C_t^3 = C_f^3 = C^3, \qquad C_f\sigma = \sigma C_f^{3m-1}$$

$$C_tC_f = C_fC_t. \tag{7}$$

From these generating equations it follows that a general element of the extended group can be represented as

$$C^{3k}C_t^uC_f^v\sigma^w, \tag{8}$$

where the limits

$$0 \leqq k \leqq m-1$$

$$0 \leqq u, v \leqq 2$$

$$0 \leqq w \leqq 1 \tag{9}$$

on the superscripts in Eq. (8) indicate that the extended group has $m \times 3 \times 3 \times 2 = 18m$ elements.

The class structure of the extended group actually depends slightly on whether m is an even or odd integer (in much the same way that the class structure for the groups C_{nv} differs for even and odd n). By using the generating equations in Eqs. (7), it can

be shown that the extended group $G_{18}^{(m)}$ contains $(9m + 3)/2$ classes when m is odd and $(9m + 6)/2$ classes when m is even. Most classes consist of two members, i.e., some particular element and its inverse. Exceptions to this rule for odd m are: the identity, which is in a class by itself, and all $9m$ elements with $w = 1$ in Eq. (8), which are in the same class. Exceptions for even m are: the identity and $C^{3m/2}$, each of which is in a class by itself, and the $9m$ elements with $w = 1$, which are distributed equally into two classes, one class for even values of $(3k + u + v)$ and one for odd values of $(3k + u + v)$ in Eq. (8).

Experimental values for ρ and values for the rational numbers p/m approximately equal to ρ are given in Table IV for four molecules. It can be seen that the extended group $G_{18}^{(m)}$ for H_3C–CD_3 is just a triple group $G_{18}^{(3)}$ of G_{18}. This simple example arises essentially because the CH and CD bond lengths are equal, while the ratio of the H and D masses is $\frac{1}{2}$. It will be described in more detail after the general group-theoretical discussion below.

We note in passing that the values of ρ given in Table IV are actually the effective values indicated by $\tilde{\rho}$ in Eq. (8a) of Ref. (*13*). The accuracy for H_3C–CF_3 (*2*) is much lower than that for the other molecules. In this case, the accuracy was limited by the nuclear hyperfine contributions to the energy splittings. With a detailed understanding of the hyperfine Hamiltonian, it should be possible to extract information on the hyperfine constants as well as to reduce substantially the error in ρ. For the other molecules, $\tilde{\rho}$ was determined entirely from anticrossings which are insensitive to the hyperfine contribution to the energy splittings. In these cases, the uncertainty in $\rho = I_{\text{top}}/(I_{\text{top}} + I_{\text{frame}})$ is determined primarily by the difference $(\tilde{\rho} - \rho)$ produced by higher order internal rotation effects (*13*). In H_3C–CD_3, this difference is $\sim$0.03% (*7, 8*).

C. *Character Tables and Symmetry Species Labels*

Tables V(a) and V(b) give the character tables for $G_{18}^{(m)}$ for odd and even values of m, respectively. These character tables take relatively simple forms and can thus probably be derived in a relatively simple fashion. In the present work, however, they were derived rather more laboriously by trial and error generation of representations using basis functions of the form $e^{\pm iKx}$, $e^{\pm is\alpha/m}$, and suitable products thereof.

When m is odd (Table V(a)), there are two nondegenerate representations A_1 and

TABLE IV

Some Values of p/m Corresponding to Experimentally Determined Values of ρ

Molecule[a]	H_3C-CF_3	H_3C-SiH_3	H_3C-SiF_3	H_3C-CD_3
ρ[b]	0.0345(3.5%)	0.3518127(0.001%)	0.02546055(0.002%)	0.3339792(0.001%)
p/m[c]	1/30 (3.4%)	13/37 (0.13%)	7/275 (0.02%)	1/3 (0.19%)

[a]The ρ values for these molecules are taken from references (2), (5), (6) and (7,8), respectively, and actually correspond to the effective values $\tilde{\rho}$ defined in Ref. (13).
[b]Numbers in parentheses represent the experimental uncertainty in percent.
[c]Numbers in parentheses represent the difference between ρ and p/m in percent.

TABLE V(a)

Character Table[a] for $G_{18}^{(m)}$ for Odd Valucs of m (See Eqs. (6)–(9))

Γ	E	[2] C^{3k} {(m-1)/2}[b]	[2] $C^{3k}C_t$ {m}[c]	[2] $C^{3k}C_f$ {m}[c]	[2] $C^{3k}C_tC_f$ {m}[c]	[2] $C^{3k}C_t^2C_f$ {m}[c]	[9m] $C^{3k}C_t^uC_f^v\sigma$
A_1	1	1	1	1	1	1	1
A_2	1	1	1	1	1	1	-1
$E_{s\tau}$	2	$2\cos 2\pi[3ks]/3m$	$2\cos 2\pi[(3k+1)s]/3m$	$2\cos 2\pi[(3k+1)s-\tau m]/3m$	$2\cos 2\pi[(3k+2)s-\tau m]/3m$	$2\cos 2\pi[(3k+3)s-\tau m]/3m$	0

[a]The number of elements in a class is given in square brackets before the representative element from that class, except when that number is unity. Classes with two members consist of an element and its inverse. The number of classes represented by a single symbol is given in curly brackets, except when that number is unity. The integer subscripts s and τ on the E species lie in the ranges $0 \leq s \leq (3m-1)/2$ and $0 \leq \tau \leq 2$, except that $E_{00} = A_1+A_2$ and $E_{01} = E_{02}$. The single-valued representations of G_{18} are A_1, A_2, E_{01}, E_{m1}, E_{m2} and E_{m0}, corresponding to A_1, A_2, E_1, E_2, E_3 and E_4, respectively, in Table II.

[b]There are (m-1)/2 classes of this type, since $1 \leq k \leq (m-1)/2$.
[c]There are m classes of this type, since $0 \leq k \leq m-1$.

TABLE V(b)

Character Table[a] for $G_{18}^{(m)}$ for Even Values of m (See Eqs. (6)–(9))

Γ	E	[2] $C^{3k}\{(m-2)/2\}$[b]	$C^{3m/2}$	[2] $C^{3k}C_t$ {m}[c]	[2] $C^{3k}C_f$ {m}[c]	[2] $C^{3k}C_tC_f$ {m}[c]	[2] $C^{3k}C_t^2C_f$ {m}[c]	[9m/2] $C^{3k}C_t{}^uC_f{}^v\sigma$ [d]	
A_1	1	1	1	1	1	1	1	1	1
A_2	1	1	1	1	1	1	1	-1	-1
B_1	1	$(-1)^k$	$(-1)^{m/2}$	$(-1)^{k+1}$	$(-1)^{k+1}$	$(-1)^k$	$(-1)^{k+1}$	1	-1
B_2	1	$(-1)^k$	$(-1)^{m/2}$	$(-1)^{k+1}$	$(-1)^{k+1}$	$(-1)^k$	$(-1)^{k+1}$	-1	1
$E_{s\tau}$	2	$2\cos 2\pi[3ks]/3m$	$2(-1)^s$	$2\cos 2\pi[(3k+1)s]/3m$	$2\cos 2\pi[(3k+1)s-\tau m]/3m$	$2\cos 2\pi[(3k+2)s-\tau m]/3m$	$2\cos 2\pi[(3k+3)s-\tau m]/3m$	0	0

[a]The number of elements in a class and the number of classes represented by a single symbol are as given in Table V(a). Classes with two members consist of an element and its inverse. The integer subscripts s and τ on the E species lie in the ranges $0 \leq s \leq 3m/2$ and $0 \leq \tau \leq 2$, except that $E_{00} = A_1+A_2$, $E_{3m/2,0} = B_1+B_2$, $E_{01} = E_{02}$ and $E_{3m/2,1} = E_{3m/2,2}$. The single-valued representations of G_{18} are as given in Table V(a).

[b]There are (m-2)/2 classes of this type, since $1 \leq k \leq (m-2)/2$. The element C^{3k} with $k = m/2$ is in a class by itself.

[c]There are m classes of this type, since $0 \leq k \leq m-1$.

[d]There are two classes of 9m/2 elements of the type $C^{3k}C_t{}^uC_f{}^v\sigma$ when m is even, one for (3k+u+v) even (left column) and one for (3k+u+v) odd (right column).

A_2, which are also single-valued representations of G_{18}. There appear at first to be $(9m + 3)/2$ doubly degenerate representations $E_{s\tau}$, since the first subscript s runs from 0 to $(3m - 1)/2$ and the second subscript τ runs from 0 to 2, but it turns out that $E_{00} = A_1 + A_2$ and $E_{01} = E_{02}$, so that in fact there are only $(9m - 1)/2$ doubly degenerate representations. The single-valued representations of G_{18} among the two-dimensional representations of $G_{18}^{(m)}$ are $E_{01} = E_1$, $E_{m1} = E_2$, $E_{m2} = E_3$, and $E_{m0} = E_4$, where the symbols after the equal signs correspond to Bunker's notation (*19*) as reproduced here in Table II.

When m is even (Table V(b)), there are four nondegenerate representations, A_1, A_2, B_1, and B_2, where the first two of these are single-valued representations of G_{18}. There appear at first to be $(9m + 6)/2$ doubly degenerate representations, since s runs from 0 to $3m/2$ and τ runs from 0 to 2, but $E_{00} = A_1 + A_2$, $E_{3m/2,0} = B_1 + B_2$, $E_{01} = E_{02}$, and $E_{3m/2,1} = E_{3m/2,2}$, so that there are actually only $(9m - 2)/2$ E species. The single-valued E representations are as given in the preceding paragraph.

The direct product of two E species (including E_{00} or $E_{3m/2,0}$) is quite easy to obtain by inspection, since it can be shown from the character tables that

$$E_{s\tau} \times E_{s'\tau'} = E_{s+s',\tau+\tau'} + E_{s-s',\tau-\tau'}. \tag{10}$$

If the subscripts on the right of Eq. (10) fall outside of the ranges specified above, they can be brought back into those ranges by noting from character Tables V(a) and V(b) that

$$E_{s,\tau} = E_{-s,-\tau} = E_{s,\tau\pm3} = E_{s\pm3m,\tau}. \tag{11}$$

The multiplication scheme of Eq. (10) can be visualized pictorially by a slight extension of the circle diagrams used to visualize various aspects of the C_{nv} groups (*20–22*). For the $G_{18}^{(m)}$ group, it is convenient to imagine *three* circles, labeled by $\tau = 0$, 1, and 2, mod 3, respectively. The species $E_{s\tau}$ is then represented by the point(s) at $\pm s(2\pi/3m)$ radians on the τ circle. The multiplication of Eq. (10) then indicates that the direct product of a point at $s(2\pi/3m)$ radians on the τ circle with a point at $s'(2\pi/3m)$ radians on the τ' circle is given by a point at $(s + s')(2\pi/3m)$ radians on the $(\tau + \tau')$ circle and a point at $(s - s')(2\pi/3m)$ radians on the $(\tau - \tau')$ circle.

As mentioned in Ref. (*12*), this pictorial representation of symmetry species by angular positions on a circle strongly suggests that the arbitrariness inherent in the choice of a particular rational number p/m as an approximation for ρ could be eliminated by working instead with some sort of continuous group. In the present formalism, for example, the symmetry species E_{p1} for (J_x, J_y) given in Table VII below corresponds to an angle of $p(2\pi/3m)$ on the circle. Since $p/m \equiv \rho$, this symmetry species would correspond to an angle of $2\pi\rho/3$ in the continuous group formalism. The appropriate continuous groups almost certainly exist in the mathematical literature, but they have not yet been searched for by the present authors.

D. Standard Forms for the Representation Matrices

Before using group theory to write down wavefunctions and operators of definite symmetry species, it is convenient to go beyond the information given in character Tables V(a) and V(b) and to choose standard forms for the various two-dimensional

irreducible representation matrices. If we label the two functions spanning a given representation $E_{s\tau}$ as $|E_{s\tau+}\rangle$ and $|E_{s\tau-}\rangle$, or equivalently as $|E_{s\tau}\rangle$ and $|E_{-s,-\tau}\rangle$, where s and τ are both positive, then we shall require that

$$C_t\begin{bmatrix}|E_{s\tau+}\rangle\\|E_{s\tau-}\rangle\end{bmatrix}=\begin{bmatrix}e^{-2\pi is/3m} & 0\\0 & e^{+2\pi is/3m}\end{bmatrix}\begin{bmatrix}|E_{s\tau+}\rangle\\|E_{s\tau-}\rangle\end{bmatrix} \tag{12}$$

when $s \neq 0$, or we shall require that

$$C_f\begin{bmatrix}|E_{01+}\rangle\\|E_{01-}\rangle\end{bmatrix}=\begin{bmatrix}e^{+2\pi i/3} & 0\\0 & e^{2\pi i/3}\end{bmatrix}\begin{bmatrix}|E_{01+}\rangle\\|E_{01-}\rangle\end{bmatrix} \tag{13}$$

for the one doubly degenerate species with $s = 0$. We shall further require that

$$\sigma\begin{bmatrix}|E_{s\tau+}\rangle\\|E_{s\tau-}\rangle\end{bmatrix}=\begin{bmatrix}0 & +1\\+1 & 0\end{bmatrix}\begin{bmatrix}|E_{s\tau+}\rangle\\|E_{s\tau-}\rangle\end{bmatrix} \tag{14}$$

for all degenerate species. Equations (12)–(14) specify completely the form of all representation matrices.

E. Transformation Properties of Basis Set Wavefunctions

Transformation properties of the rotational wavefunctions $|KJM\rangle$ are easily determined as in Ref. (*12*) from the Eulerian angle transformations given in Table III:

$$\Gamma[|KJM\rangle, |-KJM\rangle] = E_{Kp,K\text{mod}3}. \tag{15}$$

Transformation properties of trigonometric functions of the torsional angle α can also easily be determined from Table III:

$$\Gamma[\cos(\alpha s/m), \sin(\alpha s/m)] = \Gamma[e^{\pm i\alpha s/m}] = E_{s0}. \tag{16}$$

From a treatment very similar to that leading to Eqs. (22)–(24) of Ref. (*12*) we find for the ground torsional state in the high-barrier limit (i.e., in the limit of nearest-neighbor tunneling only) that torsional wavefunctions of species E_{s0} correspond to internal rotation splitting energies of

$$2X_1\cos(2\pi s/3m), \tag{17}$$

where X_1 is the nearest-neighbor tunneling matrix element.

The torsional wavefunctions used in Refs. (*1–8, 13*) can be written (*16*)

$$M_{v,K,\sigma} = e^{i\alpha(\sigma-\rho K)}U_{v,K,\sigma}, \tag{18}$$

where

$$U_{v,K,\sigma} = \sum_{k=-\infty}^{\infty} A_{3k+\sigma}^{vK}e^{3ik\alpha}. \tag{19}$$

Here v specifies the number of torsional quanta excited and $\sigma = 0, +1, -1$ labels the torsional sublevel. Except when $K = \sigma = 0$, the functions $[U_{v,K,\sigma}, U_{v,-K,-\sigma}]$ transform as $[A_1 + A_2]$. For the $K = \sigma = 0$ case, $U_{v,K,\sigma} \equiv U_{v,-K,-\sigma}$, and there is only one function, which transforms as A_1 for even v and as A_2 for odd v. Furthermore, except for $K = \sigma$

$= 0$, $[e^{\pm i\alpha(\sigma-\rho K)}]$ transforms as $E_{(\sigma m-Kp),0}$. For $K = \sigma = 0$, there is only one such function, which transforms as A_1. It follows then that, except for $K = \sigma = 0$, $[M_{v,K,\sigma}, M_{v,-K,-\sigma}]$ have the same transformation properties as $[e^{\pm i\alpha(\sigma-\rho K)}]$. For $K = \sigma = 0$, the same relationship holds, provided v is even; in particular, it holds for the ground torsional state. For $K = \sigma = 0$ and v odd, the $M_{v,0,0}$ transform as the $U_{v,0,0}$. The transformation properties of the torsional functions can thus be understood by considering only the exponential factors in Eq. (18), provided one makes proper allowance for the case with $K = \sigma = 0$ and v odd. From this discussion and Eqs. (16) and (17), it follows that $s/m = (\sigma - Kp/m) = (\sigma - K\rho)$, and $\tau = 0$ for the torsional wavefunctions in Eqs. (18) and (19), where s is to be kept in the desired range by using Eq. (11).

The symmetry species of nuclear-spin functions characterized by laboratory-fixed projections of the angular momenta can also be determined easily by direct application of the permutation-inversion operations. If we use the notation $|M_1, M_2, M_3\rangle$ for nuclei in the top and $|M_4, M_5, M_6\rangle$ for nuclei in the frame, then for nuclei of spin $\frac{1}{2}$ located in the top we find the symmetry species

$$\Gamma[|{+}{+}{+}\rangle] = A_1$$

$$\Gamma\{[|{-}{+}{+}\rangle + e^{\pm 2\pi i/3}|{+}{-}{+}\rangle + e^{\mp 2\pi i/3}|{+}{+}{-}\rangle]/\sqrt{3}\} = E_{m1}, \qquad (20)$$

where $|{-}{+}{+}\rangle$ is a shorthand notation for $|M_1 = -\frac{1}{2}, M_2 = +\frac{1}{2}, M_3 = +\frac{1}{2}\rangle$, etc., and where upper and lower sign choices correspond to wavefunctions transforming like $|E_{m1\pm}\rangle$ in Eqs. (12)–(14). The A_1 and E functions correspond to a total nuclear spin I in the top of $I_t = \frac{3}{2}$ and $I_t = \frac{1}{2}$, respectively. Other functions belonging to the same total spin I_t in the top and same symmetry species can be generated (*23*) using the ladder operator $(I_1 + I_2 + I_3)_X - i(I_1 + I_2 + I_3)_Y$.

Similarly, for nuclei of spin $\frac{1}{2}$ located in the frame, the species corresponding to the functions in Eqs. (20) are A_1 and E_{01} ($|E_{01\mp}\rangle$), respectively. The A_1 and E species correspond to a total nuclear spin in the frame of $I_f = \frac{3}{2}$ and $I_f = \frac{1}{2}$, and the ladder operator $(I_4 + I_5 + I_6)_X - i(I_4 + I_5 + I_6)_Y$ can be used to generate other functions with the same total I_f and same symmetry species. For nuclei of spin 1 located in the frame, we find

$$\Gamma[|{+}{+}{+}\rangle] = A_1$$

$$\Gamma\{[|0{+}{+}\rangle + e^{\pm 2\pi i/3}|{+}0{+}\rangle + e^{\mp 2\pi i/3}|{+}{+}0\rangle]/\sqrt{3}\} = E_{01}$$

$$\Gamma\{a[|{-}{+}{+}\rangle + e^{\pm 2\pi i/3}|{+}{-}{+}\rangle + e^{\mp 2\pi i/3}|{+}{+}{-}\rangle]/\sqrt{3}$$

$$+ b[|{+}00\rangle + e^{\pm 2\pi i/3}|0{+}0\rangle + e^{\mp 2\pi i/3}|00{+}\rangle]/\sqrt{3}\} = E_{01}$$

$$\Gamma\{c[|{-}{+}{+}\rangle + |{+}{-}{+}\rangle + |{+}{+}{-}\rangle]/\sqrt{3} + d[|{+}00\rangle + |0{+}0\rangle + |00{+}\rangle]/\sqrt{3}\} = A_1$$

$$\Gamma\{[|0{+}{-}\rangle - |0{-}{+}\rangle + |{-}0{+}\rangle - |{-}{+}0\rangle + |{+}{-}0\rangle - |{+}0{-}\rangle]/\sqrt{6}\} = A_2, \qquad (21)$$

where $|0{+}{-}\rangle$ in Eqs. (21) is a shorthand notation for $|M_4 = 0, M_5 = +1, M_6 = -1\rangle$, etc., and upper and lower sign choices correspond to wavefunctions transforming like $|E_{01\mp}\rangle$. For suitable choices of a, b, c, and d (*23*), the functions above correspond in decreasing order to $|I_f, M_f\rangle = |3, 3\rangle, |2, 2\rangle, |1, 1\rangle, |1, 1\rangle$, and $|0, 0\rangle$, respectively. The ladder operator $(I_4 + I_5 + I_6)_X - i(I_4 + I_5 + I_6)_Y$ can again be used to generate other functions with the same total I_f and symmetry species. Note that for nuclei of

spin 1, there exist functions with the same symmetry species, but with different values of I_f, i.e., $\Gamma = E_{01}$ with $I_f = 1$ or 2 and $\Gamma = A_1$ with $I_f = 1$ or 3. Thus, I_f will not, in general, be a good quantum number, and the actual form of the spin functions will depend on the magnitude of the nuclear hyperfine interactions.

The $2I + 1$ multiplicities of the nuclear-spin wavefunctions, together with the symmetry species multiplication properties and the fact that Pauli-allowed overall wavefunctions belong to either the A_1 or the A_2 species of G_{18} (regardless of the value of the nuclear spin for the individual nuclei), can be used to obtain statistical weights for the overall torsion–rotation levels. For molecules like H_3C–SiH_3 these are given in Table B-4 of Ref. (*11*): $A_1(16)$, $A_2(16)$, $E_{01}(16)$, $E_{m1}(16)$, $E_{m2}(8)$, and $E_{m0}(8)$. For H_3C–CD_3, the corresponding statistical weights are: $A_1(44)$, $A_2(44)$, $E_{01}(64)$, $E_{31}(44)$, $E_{32}(32)$, and $E_{30}(32)$.

F. Simple Example: H_3C–CD_3

We close this section by examining briefly as an example the triple group $G_{18}^{(3)}$ formalism for 1,1,1-trideuteroethane. Table VI gives the full character table for $G_{18}^{(3)}$.

For this group, $p = 1$ and $m = 3$, so that symmetry species of the symmetric-top rotational functions $|KJM\rangle$ for even J and for K values from 0 to 9 are: A_1, E_{11}, E_{22}, $E_{33} \equiv E_{30}$, $E_{44} \equiv E_{41}$, $E_{55} \equiv E_{41}$, $E_{66} \equiv E_{30}$, $E_{77} \equiv E_{22}$, $E_{88} \equiv E_{11}$, and $E_{99} \equiv A_1 + A_2$, respectively. For odd J, the $K = 0$ species is A_2. For $K > 9$, use the species given for the same K mod 9.

Symmetry species for the torsional components of H_3C–CD_3 split by internal rotation tunneling in the ground torsional state and also the correct linear combinations of the wavefunctions localized in individual wells in the threefold extended ($m = 3$) nine-well formalism can be found in Fig. 4 of Ref. (*12*). (The species E_r there corresponds to E_{r0} here.) Relative energies for these components, under the approximation that only nearest-neighbor tunneling between wells is taken into account (i.e., only $X_1 \neq 0$ in Fig. 4 of Ref. (*12*)), are shown in Fig. 2 here, using a convenient geometrical construction (*20*).

Torsion–rotation symmetry species are also shown in Fig. 2. Note, however, that the subscript τ on the representations $E_{s\tau}$ for molecules like H_3C–CD_3 does not play exactly the same role as the quantity σ does for methyl top rotations about asymmetric rotor frames (essentially because the integers $\sigma = 0, \pm 1$ are sufficient to characterize all representations of the cyclic group of order three, but are not sufficient to characterize all representations of the direct product of two cyclic groups of order three). Nevertheless, as indicated in the discussion above, a knowledge of K and σ permits one to obtain K, s, and τ, and vice versa.

When the high-barrier limit is relaxed somewhat, next-nearest, next-next-nearest neighbor tunnelings, etc., become important, and several terms are required in the energy expression sum of Eq. (24) of Ref. (*12*) or Eq. (16) of Ref. (*13*). We note in passing that even in this intermediate barrier case, many of the degeneracies exhibited in adjacent $K \neq 0$ mod 3 energy stacks of Fig. 2 will persist.

For some additional discussion and an excellent experimental illustration of these matters, the reader is referred to a recent Raman study of torsional overtones in CH_3CD_3 (*24*).

TABLE VI

The Triple Group $G_{18}^{(3)}$ of the Permutation-Inversion Group G_{18}, as Appropriate for $H_3C{-}CD_3$[a]

Γ	E	$2C^3$	$2C_t$	$2C^3C_t$	$2C^6C_t$	$2C_f$	$2C^3C_f$	$2C^6C_f$	$2C_tC_f$	$2C^3C_tC_f$	$2C^6C_tC_f$	$2C_t^2C_f$	$2C^3C_t^2C_f$	$2C^6C_t^2C_f$	$27C^{3k}C_t^uC_f^v\sigma$		Γ(G_{18})
A_1	1	1	1	1	1	1	1	1	1	1	1	1	1	1	1	μ_z	A_1
A_2	1	1	1	1	1	1	1	1	1	1	1	1	1	1	-1	μ_Z, J_z	A_2
E_{10}	2	-1	2c1	2c4	2c2	2c1	2c4	2c2	2c2	2c4	2c1	-1	-1	2	0		
E_{20}	2	-1	2c2	2c1	2c4	2c2	2c1	2c4	2c4	2c1	2c2	-1	-1	2	0		
E_{30}	2	2	-1	-1	-1	-1	-1	-1	-1	-1	-1	2	2	2	0		E_4
E_{40}	2	-1	2c4	2c2	2c1	2c4	2c2	2c1	2c1	2c2	2c4	-1	-1	2	0		
E_{01}	2	2	2	2	2	-1	-1	-1	-1	-1	-1	-1	-1	-1	0		E_1
E_{11}	2	-1	2c1	2c4	2c2	2c2	2c1	2c4	2c1	2c2	2c4	2	-1	-1	0	$(\mu_x,\mu_y),(J_x,J_y)$	
E_{21}	2	-1	2c2	2c1	2c4	2c1	2c4	2c2	2c1	2c2	2c4	-1	2	-1	0		
E_{31}	2	2	-1	-1	-1	2	2	2	-1	-1	-1	-1	-1	-1	0		E_2
E_{41}	2	-1	2c4	2c2	2c1	2c1	2c4	2c2	2c4	2c1	2c2	2	-1	-1	0		
E_{12}	2	-1	2c1	2c4	2c2	2c4	2c2	2c1	2c4	2c1	2c2	-1	2	-1	0		
E_{22}	2	-1	2c2	2c1	2c4	2c4	2c2	2c1	2c2	2c4	2c1	2	-1	-1	0		
E_{32}	2	2	-1	-1	-1	-1	-1	-1	2	2	2	-1	-1	-1	0		E_3
E_{42}	2	-1	2c4	2c2	2c1	2c2	2c1	2c4	2c2	2c4	2c1	-1	2	-1	0		

[a]The symbols c1, c2 and c4 in the body of the table represent cos40°, cos80° and cos160°, respectively. The number of elements in a class and a representative element of each class is given at the top of each column. Symmetry species for components of the dipole moment operator and total angular momentum operator are given on the right of the table, as well as the single-valued species of the permutation-inversion group G_{18} in Table II.

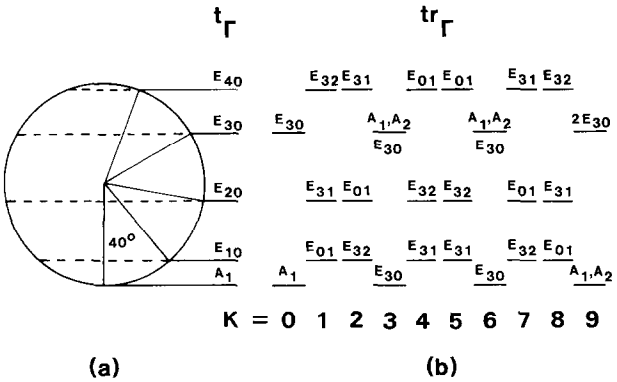

FIG. 2. (a) Torsional energy level splittings and torsional symmetry species ${}^{t}\Gamma$ for the ninefold well of $G_{18}^{(3)}$, as appropriate for H_3C–CD_3. The energy scale is arbitrary. The ratios of the splittings apply to a torsional level deep in a high-barrier well, but even in the intermediate-barrier case, many of the degeneracies exhibited in adjacent $K \neq 0$ mod 3 energy stacks will persist. The symmetry species correspond to even J and even torsional quantum number v. The species ${}^{t}\Gamma = E_{r0}$ here correspond to wavefunctions of species E_r in Fig. 4 of Ref. (*12*). (b) Torsional splittings as a function of the projection K of the total angular momentum along the symmetric-top axis (on the same scale as (a)). Note that permissible torsion–rotation symmetry species ${}^{tr}\Gamma$ in $G_{18}^{(3)}$ all correspond to single-valued representations of G_{18} in Table II.

3. SPIN–ROTATION AND SPIN–SPIN CONTRIBUTIONS TO THE HYPERFINE HAMILTONIAN

A. Symmetry Species of Laboratory-Fixed Vector Components

The symmetry species of the laboratory-fixed components of many vector operators, including the total electric dipole moment $\boldsymbol{\mu}$ of the molecule, the total angular momentum $\mathbf{J}$ of the molecule exclusive of nuclear spin, and the nuclear-spin operators $\mathbf{I}_i$ for each atom i, do not depend on which component (i.e., X, Y, or Z) is considered, and this fact is reflected in the shorthand notation below. Particles 1, 2, and 3 are taken to belong to the top (sub- or superscript t); and particles 4, 5, and 6 to the frame (sub- or superscript f). Since the permutation-inversion operations can be applied directly to the laboratory-fixed components of the various operators, it is easy to show that

$$\begin{aligned}
\Gamma[(\boldsymbol{\mu})_{X,Y,\text{or}Z}] &= A_2 \\
\Gamma[(\mathbf{J})_{X,Y,\text{or}Z}] &= A_1 \\
\Gamma[(\mathbf{I}_1 + \mathbf{I}_2 + \mathbf{I}_3)_{X,Y,\text{or}Z}] &= A_1 \\
\Gamma[(\mathbf{I}_4 + \mathbf{I}_5 + \mathbf{I}_6)_{X,Y,\text{or}Z}] &= A_1 \\
\Gamma[(\mathbf{I}_1 + e^{\pm 2\pi i/3}\mathbf{I}_2 + e^{\mp 2\pi i/3}\mathbf{I}_3)_{X,Y,\text{or}Z}] &= E_{m1} \\
\Gamma[(\mathbf{I}_4 + e^{\pm 2\pi i/3}\mathbf{I}_5 + e^{\mp 2\pi i/3}\mathbf{I}_6)_{X,Y,\text{or}Z}] &= E_{01},
\end{aligned} \tag{22}$$

where the upper and lower signs in the last of Eqs. (22) correspond to operators which transform like the functions $|E_{m1\pm}\rangle$ and $|E_{01\mp}\rangle$, respectively, in Eqs. (12)–(14).

B. Symmetry Species of Molecule-, Top-, and Frame-Fixed Vector Components

The easiest way to derive the transformation properties of vector operator components taken along axes other than the laboratory-fixed XYZ axes is to consider the transformation properties of the appropriate direction cosine matrix elements, since the transformation properties of the latter can be determined easily by direct substitution from the transformations of Eqs. (6) and Table III. If **V** is used to represent an arbitrary vector, and the subscripts L, M, t, and f are used to indicate laboratory, molecule, top, and frame components, respectively, then inspection of Eqs. (1) and (2) leads to the following transformation equations:

$$\begin{aligned}
[\mathbf{V}]_M &= S^{+1}(\chi, \theta, \phi)\cdot[\mathbf{V}]_L \\
[\mathbf{V}]_t &= S^{+1}(\chi - \rho\alpha + \alpha, \theta, \phi)\cdot[\mathbf{V}]_L \\
[\mathbf{V}]_f &= S^{+1}(\chi - \rho\alpha, \theta, \phi)\cdot[\mathbf{V}]_L. \qquad (23)
\end{aligned}$$

Symmetry species of vector components determined from the transformation properties of Eqs. (23) are given in Table VII. It is interesting to note that when the x, y components of these vector operators are taken in the top-fixed or frame-fixed axis system, the symmetry species are all single-valued representations of G_{18}, but when the x, y components are taken in the molecule-fixed system, the symmetry species can be multiple-valued representations of G_{18}. This fact agrees with the expectation that in a principal-axis-method treatment, where only top- and frame-fixed coordinate systems occur, the use of the extended-group formalism is unnecessary. (One should, however, take care not to identify all aspects of a PAM treatment with the current use of top-

TABLE VII

Symmetry Species of Various Vector Operator Components

Operator[a]	LAB[b]	MOLECULE[c]	top[d]	frame[e]
$\mu_{x,y}$	$2A_2$	E_{p1}	E_{m1}	E_{01}
μ_z	A_2	A_1	A_1	A_1
$J_{x,y}$ and $(I_1+I_2+I_3)_{x,y}$[f]	$2A_1$	E_{p1}	E_{m1}	E_{01}
J_z and $(I_1+I_2+I_3)_z$[f]	A_1	A_2	A_2	A_2
$(I_1 + e^{\pm 2\pi i/3}I_2 + e^{\mp 2\pi i/3}I_3)_{x,y}$	$2E_{m1}$	$E_{m+p,2} + E_{m-p,0}$	$A_1 + A_2 + E_{m1}$	$E_{m0} + E_{m2}$
$(I_1 + e^{\pm 2\pi i/3}I_2 + e^{\mp 2\pi i/3}I_3)_z$	E_{m1}	E_{m1}	E_{m1}	E_{m1}
$(I_4 + e^{\pm 2\pi i/3}I_5 + e^{\mp 2\pi i/3}I_6)_{x,y}$	$2E_{01}$	$E_{p0} + E_{p2}$	$E_{m0} + E_{m2}$	$A_1 + A_2 + E_{01}$
$(I_4 + e^{\pm 2\pi i/3}I_5 + e^{\mp 2\pi i/3}I_6)_z$	E_{01}	E_{01}	E_{01}	E_{01}

[a] $\mu_{x,y}$ is shorthand notation for μ_x, μ_y etc.
[b] Laboratory-fixed components, from Eqs. (22).
[c] Molecule-fixed components, from the first of Eqs. (23).
[d] Top-fixed components, from the second of Eqs. (23).
[e] Frame-fixed components, from the third of Eqs. (23).
[f] $(I_4+I_5+I_6)_{x,y}$ transforms like $(I_1+I_2+I_3)_{x,y}$ and $(I_4+I_5+I_6)_z$ transforms like $(I_1+I_2+I_3)_z$.

TABLE VIII

Tansformation Properties under the Generating Operations[a] for $G_{18}^{(m)}$ of Vector Operators with Components[b] Taken in Various Axis Systems[c]

	C_t	C_f	σ
$(I_L^t)_{q;\beta}$	$e^{-2\pi iq/3}\,(I_L^t)_{q;\beta}$	$+(I_L^t)_{q;\beta}$	$+(I_L^t)_{-q;\beta}$
$(I_M^t)_{q;\beta}$	$e^{-2\pi i(qm-\beta p)/3m}\,(I_M^t)_{q;\beta}$	$e^{-2\pi i(\beta m-\beta p)/3m}\,(I_M^t)_{q;\beta}$	$-(I_M^t)_{-q;-\beta}$
$(I_t^t)_{q;\beta}$	$e^{-2\pi i(q-\beta)/3}\,(I_t^t)_{q;\beta}$	$+(I_t^t)_{q;\beta}$	$-(I_t^t)_{-q;-\beta}$
$(I_f^t)_{q;\beta}$	$e^{-2\pi iq/3}\,(I_f^t)_{q;\beta}$	$e^{-2\pi i\beta/3}\,(I_f^t)_{q;\beta}$	$-(I_f^t)_{-q;-\beta}$
$(I_L^f)_{q;\beta}$	$+(I_L^f)_{q;\beta}$	$e^{-2\pi iq/3}\,(I_L^f)_{q;\beta}$	$+(I_L^f)_{-q;\beta}$
$(I_M^f)_{q;\beta}$	$e^{+2\pi i\beta p/3m}\,(I_M^f)_{q;\beta}$	$e^{-2\pi i(qm+\beta m-\beta p)/3m}\,(I_M^f)_{q;\beta}$	$-(I_M^f)_{-q;-\beta}$
$(I_t^f)_{q;\beta}$	$e^{+2\pi i\beta/3}\,(I_t^f)_{q;\beta}$	$e^{-2\pi iq/3}\,(I_t^f)_{q;\beta}$	$-(I_t^f)_{-q;-\beta}$
$(I_f^f)_{q;\beta}$	$+(I_f^f)_{q;\beta}$	$e^{-2\pi i(q+\beta)/3}\,(I_f^f)_{q;\beta}$	$-(I_f^f)_{-q;-\beta}$

[a]The generating operations C_t, C_f and σ are defined in Table III.
[b]The subscripts q and β are defined in Eqs. (24-25).
[c]Molecule-fixed (M), top-fixed (t) and frame-fixed (f) vector components are defined in terms of the laboratory-fixed (L) components in Eqs. (23).

and frame-fixed axis systems. While the axis systems in a PAM treatment are the same as the top- and frame-fixed systems used here, the operators in a PAM treatment do not have precisely the same definitions as those in an IAM treatment.)

For the purpose of constructing contributions to the hyperfine Hamiltonian of definite symmetry species, we shall make repeated use of a convenient but slightly cumbersome notation similar to that used for a hyperfine treatment in ^2E electronic states of C_{3v} molecules (*25*). Three linearly independent combinations (specified by a subscript q = 0, ±1) of the individual nuclear-spin operators in the top or frame (specified by a superscript t or f) are defined by

$$(\mathbf{I}^t)_q \equiv \mathbf{I}_1 + e^{+2\pi iq/3}\mathbf{I}_2 + e^{-2\pi iq/3}\mathbf{I}_3$$
$$(\mathbf{I}^f)_q \equiv \mathbf{I}_4 + e^{+2\pi iq/3}\mathbf{I}_5 + e^{-2\pi iq/3}\mathbf{I}_6. \tag{24}$$

Vector components are then specified by a subscript L, M, t, or f, which indicates the axis system, together with a subscript β,

$$(\mathbf{I}^t_{L,M,t,f})_{q;\beta} \equiv [(\mathbf{I}^t)_q]_\beta$$
$$(\mathbf{I}^f_{L,M,t,f})_{q;\beta} \equiv [(\mathbf{I}^f)_q]_\beta, \tag{25}$$

where $\beta = X$, Y, or Z for laboratory-fixed vector components (L), and $\beta = 0, \pm 1$ (i.e., z or $x \pm iy$) for molecule-fixed (M), top-fixed (t), or frame-fixed (f) vector components. Transformation properties of various vector operators in the notation of Eqs. (25) are given in Table VIII.

C. *The Nuclear-Spin–Overall-Rotation Operator H_{sr}*

In a normal point group treatment we would at this point seek, as possible symmetry allowed contributions to H_{sr}, all totally symmetric products of the rotational and nuclear spin operators which are linear in both the components of **J** and the components of the $\mathbf{I}_i$. In the present treatment, we seek instead all bilinear products, *which can be made totally symmetric by multiplication with an appropriate function of the internal rotation angle* α. Since the trigonometric functions of α all belong to one of the species E_{s0} (i.e., all have $\tau = 0$), we seek products linear in **J** and in the components of the $\mathbf{I}_i$ which also belong to the species E_{s0}. Bilinear products of **J** and $\mathbf{I}_i$ of species A_1 can be used with constant coefficients as terms in H_{sr}. Products of species A_2 can be used after multiplication by $\sin 3\alpha$. Bilinear products of **J** and $\mathbf{I}_i$ of species E_{r0} can be converted to the species E_{00} (i.e., to $A_1 + A_2$) by appropriate multiplication with $\cos(r\alpha/m)$ and $\sin(r\alpha/m)$, and thus products of species E_{r0} give rise to two terms in H_{rs}. (Note that the prescription in this paragraph is essentially a procedure for counting the number of different bilinear products of **J** and the $\mathbf{I}_i$ which can be used in H_{sr}, and is not a procedure for counting the number of all possible terms in H_{sr}, since, for example, any A_1 term in H_{sr} can be used to generate an infinite number of others by multiplication with $\cos 3n\alpha$ for arbitrary integer values of n.)

There is another question which arises in this counting procedure, namely the question of which axis system the vector components should be taken in. In fact, as we shall see in the next three paragraphs, it does not actually matter; the apparent form of the operators will change in the various descriptions, but the number of allowed bilinear products of **J** and the $\mathbf{I}_i$ which can be used in H_{sr} will not.

Consider first an H_{sr} operator constructed entirely from molecule-fixed vector components. We see from Table VII that $\Gamma(\mathbf{J}) = A_2 + E_{p1}$ and that $\Gamma(\mathbf{I}_{1,2,\ldots,6}) = 2A_2 + 2E_{p1}$ plus the six symmetry species in the last four rows of the "MOLECULE" column. $\Gamma(\mathbf{J}) \times \Gamma(\mathbf{I}_{1,2,\ldots,6})$ then contains the following species with $\tau = 0$: $2A_1 + 2E_{00} + 2E_{p0} + 2E_{m-p,0} + E_{2p,0} + E_{m+2p,0}$. The species A_1 is contained in this set four times, and the corresponding four operators can be used directly in H_{sr}; i.e., they can be used with constant coefficients. By multiplication with suitable functions of α, 14 other A_1 terms can be constructed, so that the total number of different terms for H_{sr} is 18 (where two terms are *not* considered to be different if they can be written in the form $g(\alpha) \cdot f(\alpha, \mathbf{I}_i, \mathbf{J})$ and $h(\alpha) \cdot f(\alpha, \mathbf{I}_i, \mathbf{J})$).

Consider next an H_{sr} operator constructed entirely from top-fixed vector components. Again from Table VII, $\Gamma(\mathbf{J}) = A_2 + E_{m1}$ and $\Gamma(\mathbf{I}_{1,2,\ldots,6}) = 2A_2 + 2E_{m1}$ plus the seven species in the last four rows of the "top" column. $\Gamma(\mathbf{J}) \times \Gamma(\mathbf{I}_{1,2,\ldots,6})$ then contains the following species with $\tau = 0$: $2A_1 + 5E_{00} + 3E_{m0}$. The seven A_1 terms can be used directly in H_{sr}, and 11 other A_1 terms can be constructed by multiplication with suitable functions of α, so that a total of 18 terms for H_{sr} is again obtained.

The same total of 18 is obtained if, as another example, we use molecule-fixed components for **J**, top-fixed components for the $\mathbf{I}_i$ when $i = 1, 2, 3$, and frame-fixed components for the $\mathbf{I}_i$ when $i = 4, 5, 6$.

Even though the total number of allowed operators in H_{sr} does not depend on the axis system chosen, some choices are more convenient than others for a given purpose. Thus, to compare H_{sr} for H_3C–SiH_3 with H_{sr} for the protons in PH_3, for example, it

would be convenient to use top-fixed components for **J** and the $\mathbf{I}_i$ when $i = 1, 2, 3$ and frame-fixed components for **J** and the $\mathbf{I}_i$ when $i = 4, 5, 6$. H_{sr} for H_3C–SiH_3 will then separate into two parts

$$H_{sr} = H_{sr}^{t} + H_{sr}^{f}, \tag{26}$$

one part for the protons in the top, the other for the protons in the frame, and each of these parts should individually have the same form as H_{sr} for the protons in PH_3. On the other hand, when taking matrix elements in an IAM basis set, it would be convenient to use molecule-fixed components for all vector operators, since then the conversion of the nuclear-spin angular momenta to laboratory-fixed components involves direction cosine matrix elements which are functions only of the rotational angles. Table IX presents the symmetry-allowed contributions to H_{sr} in both of the forms described in this paragraph.

The five α-independent terms for either H_{sr}^{t} or H_{sr}^{f} which can be obtained by setting $n = 0$ on the right-hand side of Table IX correspond to the five spin–rotation operators allowed for the protons in a C_{3v} molecule like PH_3 (*27*). In practice, consideration is usually limited to the three such operators having selection rules $\Delta K = 0, \pm 2$ (i.e., to the operators in the first, second, and fifth rows of either H_{sr}^{t} or H_{sr}^{f}) by using a diagonal spin–rotation coupling tensor (*27, 28*). The local environment of a given H atom in PH_3 actually has only a plane of symmetry, however, so that for an H atom lying in the xz plane, for example, the two additional products $J_x I_z$ and $J_z I_x$, which have selection rules $\Delta K = \pm 1$, are also permitted by symmetry considerations to occur in H_{sr}. Spin–rotation (and spin–spin) hyperfine matrix elements off-diagonal in K are described in some detail in the Appendix of Ref. (*3*).

The spin–rotation operators in Table IX can be converted to a form convenient for $\Delta J = 0$ matrix elements in a basis set containing nuclear-spin functions characterized by laboratory-fixed projection quantum numbers by using the operator equivalent

$$(I_M)_{q;\beta}(J_M)_{\beta'} \rightarrow [(\mathbf{I}_L)_q \cdot (\mathbf{J}_L)][(J_M)_\beta (J_M)_{\beta'}/J(J+1)]. \tag{27}$$

For $\Delta J = \pm 1$ matrix elements, more complicated ladder operator (*23*) or spherical tensor (*29–32*) techniques prove convenient. The procedure developed by Bowater *et al.* (*30*), in which spherical tensor expressions are applied only after the molecule-fixed components of all vector operators have been converted to laboratory-fixed components multiplied by the direction cosine matrix (as in Eqs. (23) above), is to be recommended here also (after modification to include the torsional angle α), as an excellent means for avoiding the introduction of phase-factor and sign-convention errors when applying standard vector coupling and spherical tensor techniques to angular momenta obeying commutation relations with the anomalous sign of i (*26*). In particular, $(\mathbf{I}_M)_q$ and $\mathbf{J}_M$ here represent *three* pairs (*31, 32*) of analogs ($q = 0, \pm 1$) of **S** and **N** in Eq. (9) of Ref. (*30*), while $(\mathbf{I}_L)_q$ and $\mathbf{J}_L$ represent three pairs of analogs of **S** and **N** in Eq. (30) there.

D. The Nuclear-Spin–Internal-Rotation Operator H_{sir}

The symmetry species Γ of the torsional momentum p_α is the same in the molecule-, top-, and frame-fixed axis systems and is given by

TABLE IX

Symmetry Allowed Terms[a] in the Spin–Rotation Operator $H_{sr} = H_{sr}^{t} + H_{sr}^{f}$

Molecule-fixed components	$H_{sr}{}^{t}$	Top-fixed components[b]
$(e^{-3ni\alpha} + e^{+3ni\alpha})(I_M{}^t)_{0;z}(J_M)_z$		$(e^{-3ni\alpha} + e^{+3ni\alpha})(I_t{}^t)_{0;z}(J_t)_z$
$e^{-3ni\alpha}\ \{(I_M{}^t)_{0;-},(J_M)_+\} + e^{+3ni\alpha}\ \{(I_M{}^t)_{0;+},(J_M)_-\}$		$e^{-3ni\alpha}\ \{(I_t{}^t)_{0;-},(J_t)_+\} + e^{+3ni\alpha}\ \{(I_t{}^t)_{0;+},(J_t)_-\}$
$e^{-3ni\alpha-i\alpha(m-p)/m}\ \{(I_M{}^t)_{+;z},(J_M)_+\} + e^{+3ni\alpha+i\alpha(m-p)/m}\ \{(I_M{}^t)_{-;z},(J_M)_-\}$		$e^{-3ni\alpha}\ \{(I_t{}^t)_{+;z},(J_t)_+\} + e^{+3ni\alpha}\ \{(I_t{}^t)_{-;z},(J_t)_-\}$
$e^{-3ni\alpha-i\alpha(m-p)/m}\ \{(I_M{}^t)_{+;+},(J_M)_z\} + e^{+3ni\alpha+i\alpha(m-p)/m}\ \{(I_M{}^t)_{-;-},(J_M)_z\}$		$e^{-3ni\alpha}\ \{(I_t{}^t)_{+;+},(J_t)_z\} + e^{+3ni\alpha}\ \{(I_t{}^t)_{-;-},(J_t)_z\}$
$e^{-3ni\alpha-2i\alpha(m-p)/m}\ (I_M{}^t)_{-;+}(J_M)_+ + e^{+3ni\alpha+2i\alpha(m-p)/m}\ (I_M{}^t)_{+;-}(J_M)_-$		$e^{-3ni\alpha}\ (I_t{}^t)_{-;+}(J_t)_+ + e^{+3ni\alpha}\ (I_t{}^t)_{+;-}(J_t)_-$
Molecule-fixed components	$H_{sr}{}^{f}$	**Frame-fixed components[b]**
$(e^{-3ni\alpha} + e^{+3ni\alpha})(I_M{}^f)_{0;z}(J_M)_z$		$(e^{-3ni\alpha} + e^{+3ni\alpha})(I_f{}^f)_{0;z}(J_f)_z$
$e^{-3ni\alpha}\ \{(I_M{}^f)_{0;-},(J_M)_+\} + e^{+3ni\alpha}\ \{(I_M{}^f)_{0;+},(J_M)_-\}$		$e^{-3ni\alpha}\ \{(I_f{}^f)_{0;-},(J_f)_+\} + e^{+3ni\alpha}\ \{(I_f{}^f)_{0;+},(J_f)_-\}$
$e^{-3ni\alpha+i\alpha p/m}\ \{(I_M{}^f)_{-;z},(J_M)_+\} + e^{+3ni\alpha-i\alpha p/m}\ \{(I_M{}^f)_{+;z},(J_M)_-\}$		$e^{-3ni\alpha}\ \{(I_f{}^f)_{-;z},(J_f)_+\} + e^{+3ni\alpha}\ \{(I_f{}^f)_{+;z},(J_f)_-\}$
$e^{-3ni\alpha+i\alpha p/m}\ \{(I_M{}^f)_{-;+},(J_M)_z\} + e^{+3ni\alpha-i\alpha p/m}\ \{(I_M{}^f)_{+;-},(J_M)_z\}$		$e^{-3ni\alpha}\ \{(I_f{}^f)_{-;+},(J_f)_z\} + e^{+3ni\alpha}\ \{(I_f{}^f)_{+;-},(J_f)_z\}$
$e^{-3ni\alpha+2i\alpha p/m}\ (I_M{}^f)_{+;+}(J_M)_+ + e^{+3ni\alpha-2i\alpha p/m}\ (I_M{}^f)_{-;-}(J_M)_-$		$e^{-3ni\alpha}\ (I_f{}^f)_{+;+}(J_f)_+ + e^{+3ni\alpha}\ (I_f{}^f)_{-;-}(J_f)_-$

[a]See Eqs. (23-25) and Table VIII. Operators with different α dependence can be obtained by choosing any positive or negative integer value for n, but only 18 different operators can be constructed if operators of the form $g(\alpha)\cdot f(\alpha,\mathbf{I}_i,\mathbf{J})$ and $h(\alpha)\cdot f(\alpha,\mathbf{I}_i,\mathbf{J})$ are not counted separately. $\{A,B\} \equiv AB + BA$ is used for operators which do not commute (26).

[b]Operators independent of α can be obtained by taking n = 0. These correspond to H_{sr} for the protons in PH_3 (27).

$$\Gamma(p_\alpha) = A_2. \tag{28}$$

Because p_α transforms like J_z, nuclear-spin–internal-rotation interaction operators can be constructed from the nuclear-spin–overall-rotation operators in Table IX by replacing $(J_M)_z$, $(J_t)_z$, or $(J_f)_z$ by p_α, and then making the resulting term Hermitian ($[p_\alpha, e^{ik\alpha}] \neq 0$).

In the intermediate- and high-barrier cases, expectation values of the form $\langle vK\sigma | p_\alpha | vK\sigma \rangle$ are rather small for low v, i.e., of the order of 0.001, 0.03, and 0.5 for $v = 0$, 1, and 2 in the molecules of interest in this paper, so that at least for $v = 0$, these nuclear-spin–internal-rotation interaction terms can probably safely be ignored.

The nuclear-spin–internal-rotation interaction terms provide a convenient illustration of the advantages of the IAM system for relatively high-barrier problems. Consider, for example, spin–rotation and spin–internal-rotation operators of the following form for nuclei in the top (t):

$$H_{\mathrm{IAM}} = c_t^p (I_M^t)_{0;z} (p_\alpha)_{\mathrm{IAM}} + c_t^J (I_M^t)_{0;z} J_z, \tag{29}$$

and

$$\begin{aligned} H_{\mathrm{PAM}} &= \bar{c}_t^p (I_M^t)_{0;z} (p_\alpha)_{\mathrm{PAM}} + \bar{c}_t^J (I_M^t)_{0;z} J_z \\ &= \bar{c}_t^p (I_M^t)_{0;z} [(p_\alpha)_{\mathrm{IAM}} + \rho J_z] + \bar{c}_t^J (I_M^t)_{0;z} J_z \\ &= \bar{c}_t^p (I_M^t)_{0;z} (p_\alpha)_{\mathrm{IAM}} + (\bar{c}_t^J + \rho \bar{c}_t^p)(I_M^t)_{0;z} J_z, \end{aligned} \tag{30}$$

where $(\mathbf{I}^t)_0 \equiv (\mathbf{I}_1 + \mathbf{I}_2 + \mathbf{I}_3)$, and where the subscripts IAM and PAM on p_α refer to operators as they are conventionally defined in these two systems (*16*). From Eqs. (29) and (30) we conclude that

$$\begin{aligned} c_t^J &\to (\bar{c}_t^J + \rho \bar{c}_t^p) \\ c_t^p &\to \bar{c}_t^p. \end{aligned} \tag{31}$$

However, expectation values of the IAM and PAM operators p_α are related by the equation

$$\langle (p_\alpha)_{\mathrm{PAM}} \rangle = \langle (p_\alpha)_{\mathrm{IAM}} \rangle + \rho \langle J_z \rangle. \tag{32}$$

Since $\langle (p_\alpha)_{\mathrm{IAM}} \rangle \to 0$ as $V_3 \to \infty$, we see that $\langle (p_\alpha)_{\mathrm{PAM}} \rangle \to \rho K$ as $V_3 \to \infty$. Thus, there is no clear separation of spin–rotation and spin–internal-rotation effects in the PAM system when $V_3 \to \infty$, in contrast to the IAM system, where a clear separation does occur.

E. The Nuclear-Spin–Nuclear-Spin Operator H_{ss}

Symmetry-allowed terms in H_{ss} can also be constructed using the transformation properties indicated in Table VIII. It is convenient to divide H_{ss} into three parts,

$$H_{ss} = H_{ss}^t + H_{ss}^f + H_{ss}^{tf}, \tag{33}$$

one part for interactions wholly within the top, one for interactions wholly within the frame, and one for interactions between the top and the frame nuclei. Tables X, XI, and XII give the symmetry-allowed operators occurring in these three parts of H_{ss}. If,

TABLE X

Symmetry Allowed Terms[a] in the Spin–Spin Operator H^t_{ss} Describing Interactions Wholly within the Top

Row	Molecule-fixed components	$H_{ss}{}^t$	Top-fixed components[b]
1	$(e^{-3ni\alpha} + e^{+3ni\alpha})(I_M{}^t)_{0;z}(I_M{}^t)_{0;z}$		$(e^{-3ni\alpha} + e^{+3ni\alpha})(I_t{}^t)_{0;z}(I_t{}^t)_{0;z}$
2	$(e^{-3ni\alpha} + e^{+3ni\alpha})(I_M{}^t)_{+;z}(I_M{}^t)_{-;z}$		$(e^{-3ni\alpha} + e^{+3ni\alpha})(I_t{}^t)_{+;z}(I_t{}^t)_{-;z}$
3	$(e^{-3ni\alpha} + e^{+3ni\alpha})\{(I_M{}^t)_{0;+},(I_M{}^t)_{0;-}\}$		$(e^{-3ni\alpha} + e^{+3ni\alpha})\{(I_t{}^t)_{0;+},(I_t{}^t)_{0;-}\}$
4	$(e^{-3ni\alpha} + e^{+3ni\alpha})\{(I_M{}^t)_{+;+},(I_M{}^t)_{-;-}\}$		$(e^{-3ni\alpha} + e^{+3ni\alpha})\{(I_t{}^t)_{+;+},(I_t{}^t)_{-;-}\}$
5	$(e^{-3ni\alpha} + e^{+3ni\alpha})\{(I_M{}^t)_{-;+},(I_M{}^t)_{+;-}\}$		$(e^{-3ni\alpha} + e^{+3ni\alpha})\{(I_t{}^t)_{-;+},(I_t{}^t)_{+;-}\}$
6	$e^{-3ni\alpha-i\alpha(m-p)/m}\{(I_M{}^t)_{0;+},(I_M{}^t)_{+;z}\} + e^{+3ni\alpha+i\alpha(m-p)/m}\{(I_M{}^t)_{0;-},(I_M{}^t)_{-;z}\}$		$e^{-3ni\alpha}\{(I_t{}^t)_{0;+},(I_t{}^t)_{+;z}\} + e^{+3ni\alpha}\{(I_t{}^t)_{0;-},(I_t{}^t)_{-;z}\}$
7	$e^{-3ni\alpha-i\alpha(m-p)/m}\{(I_M{}^t)_{+;+},(I_M{}^t)_{0;z}\} + e^{+3ni\alpha+i\alpha(m-p)/m}\{(I_M{}^t)_{-;-},(I_M{}^t)_{0;z}\}$		$e^{-3ni\alpha}\{(I_t{}^t)_{+;+},(I_t{}^t)_{0;z}\} + e^{+3ni\alpha}\{(I_t{}^t)_{-;-},(I_t{}^t)_{0;z}\}$
8	$e^{-3ni\alpha-i\alpha(m-p)/m}\{(I_M{}^t)_{-;+},(I_M{}^t)_{-;z}\} + e^{+3ni\alpha+i\alpha(m-p)/m}\{(I_M{}^t)_{+;-},(I_M{}^t)_{+;z}\}$		$e^{-3ni\alpha}\{(I_t{}^t)_{-;+},(I_t{}^t)_{-;z}\} + e^{+3ni\alpha}\{(I_t{}^t)_{+;-},(I_t{}^t)_{+;z}\}$
9	$e^{-3ni\alpha-2i\alpha(m-p)/m}(I_M{}^t)_{+;+}(I_M{}^t)_{+;+} + e^{+3ni\alpha+2i\alpha(m-p)/m}(I_M{}^t)_{-;-}(I_M{}^t)_{-;-}$		$e^{-3ni\alpha}(I_t{}^t)_{+;+}(I_t{}^t)_{+;+} + e^{+3ni\alpha}(I_t{}^t)_{-;-}(I_t{}^t)_{-;-}$
10	$e^{-3ni\alpha-2i\alpha(m-p)/m}(I_M{}^t)_{0;+}(I_M{}^t)_{-;+} + e^{+3ni\alpha+2i\alpha(m-p)/m}(I_M{}^t)_{0;-}(I_M{}^t)_{+;-}$		$e^{-3ni\alpha}(I_t{}^t)_{0;+}(I_t{}^t)_{-;+} + e^{+3ni\alpha}(I_t{}^t)_{0;-}(I_t{}^t)_{+;-}$

[a]See Eqs. (23-25) and Table VIII. $\{A,B\} \equiv AB+BA$. Operators with different α dependence can be obtained by choosing any positive or negative integer value for n, but only 15 different operators can be constructed, if operators of the form $g(\alpha)\cdot f(\alpha,\mathbf{I}_i,\mathbf{I}_j)$ and $h(\alpha)\cdot f(\alpha,\mathbf{I}_i,\mathbf{I}_j)$ are not counted separately.

[b]Operators independent of α can be obtained by taking $n = 0$. These correspond to H_{ss} for the protons in PH_3.

TABLE XI

Symmetry Allowed Terms[a] in the Spin–Spin Operator H_{ss}^{f} Describing Interactions Wholly within the Frame

Row	Molecule-fixed components	$H_{ss}{}^{f}$	Frame-fixed components[b]
1	$(e^{-3ni\alpha} + e^{+3ni\alpha})(I_M^f)_{0;z}(I_M^f)_{0;z}$		$(e^{-3ni\alpha} + e^{+3ni\alpha})(I_f^f)_{0;z}(I_f^f)_{0;z}$
2	$(e^{-3ni\alpha} + e^{+3ni\alpha})(I_M^f)_{+;z}(I_M^f)_{-;z}$		$(e^{-3ni\alpha} + e^{+3ni\alpha})(I_f^f)_{+;z}(I_f^f)_{-;z}$
3	$(e^{-3ni\alpha} + e^{+3ni\alpha})\{(I_M^f)_{0;+},(I_M^f)_{0;-}\}$		$(e^{-3ni\alpha} + e^{+3ni\alpha})\{(I_f^f)_{0;+},(I_f^f)_{0;-}\}$
4	$(e^{-3ni\alpha} + e^{+3ni\alpha})\{(I_M^f)_{-;+},(I_M^f)_{+;-}\}$		$(e^{-3ni\alpha} + e^{+3ni\alpha})\{(I_f^f)_{-;+},(I_f^f)_{+;-}\}$
5	$(e^{-3ni\alpha} + e^{+3ni\alpha})\{(I_M^f)_{+;+},(I_M^f)_{-;-}\}$		$(e^{-3ni\alpha} + e^{+3ni\alpha})\{(I_f^f)_{+;+},(I_f^f)_{-;-}\}$
6	$e^{-3ni\alpha+i\alpha p/m}\{(I_M^f)_{0;+},(I_M^f)_{-;z}\} + e^{+3ni\alpha-i\alpha p/m}\{(I_M^f)_{0;-},(I_M^f)_{+;z}\}$		$e^{-3ni\alpha}\{(I_f^f)_{0;+},(I_f^f)_{-;z}\} + e^{+3ni\alpha}\{(I_f^f)_{0;-},(I_f^f)_{+;z}\}$
7	$e^{-3ni\alpha+i\alpha p/m}\{(I_M^f)_{-;+},(I_M^f)_{0;z}\} + e^{+3ni\alpha-i\alpha p/m}\{(I_M^f)_{+;-},(I_M^f)_{0;z}\}$		$e^{-3ni\alpha}\{(I_f^f)_{-;+},(I_f^f)_{0;z}\} + e^{+3ni\alpha}\{(I_f^f)_{+;-},(I_f^f)_{0;z}\}$
8	$e^{-3ni\alpha+i\alpha p/m}\{(I_M^f)_{+;+},(I_M^f)_{+;z}\} + e^{+3ni\alpha-i\alpha p/m}\{(I_M^f)_{-;-},(I_M^f)_{-;z}\}$		$e^{-3ni\alpha}\{(I_f^f)_{+;+},(I_f^f)_{+;z}\} + e^{+3ni\alpha}\{(I_f^f)_{-;-},(I_f^f)_{-;z}\}$
9	$e^{-3ni\alpha+2i\alpha p/m}(I_M^f)_{-;+}(I_M^f)_{-;+} + e^{+3ni\alpha-2i\alpha p/m}(I_M^f)_{+;-}(I_M^f)_{+;-}$		$e^{-3ni\alpha}(I_f^f)_{-;+}(I_f^f)_{-;+} + e^{+3ni\alpha}(I_f^f)_{+;-}(I_f^f)_{+;-}$
10	$e^{-3ni\alpha+2i\alpha p/m}(I_M^f)_{0;+}(I_M^f)_{+;+} + e^{+3ni\alpha-2i\alpha p/m}(I_M^f)_{0;-}(I_M^f)_{-;-}$		$e^{-3ni\alpha}(I_f^f)_{0;+}(I_f^f)_{+;+} + e^{+3ni\alpha}(I_f^f)_{0;-}(I_f^f)_{-;-}$

[a] See Eqs. (23-25) and Table VIII. $\{A,B\} \equiv AB+BA$. Operators with different α dependence can be obtained by choosing any positive or negative integer value for n, but only 15 different operators can be constructed, if operators of the form $g(\alpha)\cdot f(\alpha,\mathbf{I}_i,\mathbf{I}_j)$ and $h(\alpha)\cdot f(\alpha,\mathbf{I}_i,\mathbf{I}_j)$ are not counted separately.

[b] Operators independent of α can be obtained by taking n = 0. These correspond to H_{ss} for the protons in PH_3.

TABLE XII

Symmetry Allowed Terms[a] in the Spin–Spin Operator H_{ss}^{tf} Describing Interactions between the Top and Frame

Row	Molecule-fixed components	H_{ss}^{tf}	Frame-fixed components
1	$(e^{-3ni\alpha} + e^{+3ni\alpha})(I_M^t)_{0;z}(I_M^f)_{0;z}$		$(e^{-3ni\alpha} + e^{+3ni\alpha})(I_f^t)_{0;z}(I_f^f)_{0;z}$
2	$e^{-3ni\alpha-i\alpha}(I_M^t)_{+;z}(I_M^f)_{+;z} + e^{+3ni\alpha+i\alpha}(I_M^t)_{-;z}(I_M^f)_{-;z}$		$e^{-3ni\alpha-i\alpha}(I_f^t)_{+;z}(I_f^f)_{+;z} + e^{+3ni\alpha+i\alpha}(I_f^t)_{-;z}(I_f^f)_{-;z}$
3	$e^{-3ni\alpha}(I_M^t)_{0;-}(I_M^f)_{0;+} + e^{+3ni\alpha}(I_M^t)_{0;+}(I_M^f)_{0;-}$		$e^{-3ni\alpha}(I_f^t)_{0;-}(I_f^f)_{0;+} + e^{+3ni\alpha}(I_f^t)_{0;+}(I_f^f)_{0;-}$
4	$e^{-3ni\alpha-i\alpha}(I_M^t)_{+;-}(I_M^f)_{+;+} + e^{+3ni\alpha+i\alpha}(I_M^t)_{-;+}(I_M^f)_{-;-}$		$e^{-3ni\alpha-i\alpha}(I_f^t)_{+;-}(I_f^f)_{+;+} + e^{+3ni\alpha+i\alpha}(I_f^t)_{-;+}(I_f^f)_{-;-}$
5	$e^{-3ni\alpha+i\alpha}(I_M^t)_{-;-}(I_M^f)_{-;+} + e^{+3ni\alpha-i\alpha}(I_M^t)_{+;+}(I_M^f)_{+;-}$		$e^{-3ni\alpha+i\alpha}(I_f^t)_{-;-}(I_f^f)_{-;+} + e^{+3ni\alpha-i\alpha}(I_f^t)_{+;+}(I_f^f)_{+;-}$
6	$e^{-3ni\alpha+i\alpha p/m}(I_M^t)_{0;z}(I_M^f)_{-;+} + e^{+3ni\alpha-i\alpha p/m}(I_M^t)_{0;z}(I_M^f)_{+;-}$		$e^{-3ni\alpha}(I_f^t)_{0;z}(I_f^f)_{-;+} + e^{+3ni\alpha}(I_f^t)_{0;z}(I_f^f)_{+;-}$
7	$e^{-3ni\alpha-i\alpha(m-p)/m}(I_M^t)_{+;z}(I_M^f)_{0;+} + e^{+3ni\alpha+i\alpha(m-p)/m}(I_M^t)_{-;z}(I_M^f)_{0;-}$		$e^{-3ni\alpha-i\alpha}(I_f^t)_{+;z}(I_f^f)_{0;+} + e^{+3ni\alpha+i\alpha}(I_f^t)_{-;z}(I_f^f)_{0;-}$
8	$e^{-3ni\alpha+i\alpha(m+p)/m}(I_M^t)_{-;z}(I_M^f)_{+;+} + e^{+3ni\alpha-i\alpha(m+p)/m}(I_M^t)_{+;z}(I_M^f)_{-;-}$		$e^{-3ni\alpha+i\alpha}(I_f^t)_{-;z}(I_f^f)_{+;+} + e^{+3ni\alpha-i\alpha}(I_f^t)_{+;z}(I_f^f)_{-;-}$
9	$e^{-3ni\alpha+i\alpha p/m}(I_M^t)_{0;+}(I_M^f)_{-;z} + e^{+3ni\alpha-i\alpha p/m}(I_M^t)_{0;-}(I_M^f)_{+;z}$		$e^{-3ni\alpha}(I_f^t)_{0;+}(I_f^f)_{-;z} + e^{+3ni\alpha}(I_f^t)_{0;-}(I_f^f)_{+;z}$
10	$e^{-3ni\alpha-i\alpha(m-p)/m}(I_M^t)_{+;+}(I_M^f)_{0;z} + e^{+3ni\alpha+i\alpha(m-p)/m}(I_M^t)_{-;-}(I_M^f)_{0;z}$		$e^{-3ni\alpha-i\alpha}(I_f^t)_{+;+}(I_f^f)_{0;z} + e^{+3ni\alpha+i\alpha}(I_f^t)_{-;-}(I_f^f)_{0;z}$
11	$e^{-3ni\alpha+i\alpha(m+p)/m}(I_M^t)_{-;+}(I_M^f)_{+;z} + e^{+3ni\alpha-i\alpha(m+p)/m}(I_M^t)_{+;-}(I_M^f)_{-;z}$		$e^{-3ni\alpha+i\alpha}(I_f^t)_{-;+}(I_f^f)_{+;z} + e^{+3ni\alpha-i\alpha}(I_f^t)_{+;-}(I_f^f)_{-;z}$
12	$e^{-3ni\alpha+2i\alpha p/m}(I_M^t)_{0;+}(I_M^f)_{+;+} + e^{+3ni\alpha-2i\alpha p/m}(I_M^t)_{0;-}(I_M^f)_{-;-}$		$e^{-3ni\alpha}(I_f^t)_{0;+}(I_f^f)_{+;+} + e^{+3ni\alpha}(I_f^t)_{0;-}(I_f^f)_{-;-}$
13	$e^{-3ni\alpha-i\alpha(m-2p)/m}(I_M^t)_{+;+}(I_M^f)_{-;+} + e^{+3ni\alpha+i\alpha(m-2p)/m}(I_M^t)_{-;-}(I_M^f)_{+;-}$		$e^{-3ni\alpha-i\alpha}(I_f^t)_{+;+}(I_f^f)_{-;+} + e^{+3ni\alpha+i\alpha}(I_f^t)_{-;-}(I_f^f)_{+;-}$
14	$e^{-3ni\alpha+i\alpha(m+2p)/m}(I_M^t)_{-;+}(I_M^f)_{0;+} + e^{+3ni\alpha-i\alpha(m+2p)/m}(I_M^t)_{+;-}(I_M^f)_{0;-}$		$e^{-3ni\alpha+i\alpha}(I_f^t)_{-;+}(I_f^f)_{0;+} + e^{+3ni\alpha-i\alpha}(I_f^t)_{+;-}(I_f^f)_{0;-}$

[a]See Eqs. (23-25) and Table VIII. Operators with different α dependence can be obtained by choosing any positive or negative value for the integer n, but only 27 different operators can be constructed if operators of the form $g(\alpha)\cdot f(\alpha,\mathbf{I}_i,\mathbf{I}_j)$ and $h(\alpha)\cdot f(\alpha,\mathbf{I}_i,\mathbf{I}_i)$ are not counted separately.

as for H_{sr} in Section 3C, operators of the form $g(\alpha)\cdot f(\alpha, \mathbf{I}_i, \mathbf{I}_j)$ and $h(\alpha)\cdot f(\alpha, \mathbf{I}_i, \mathbf{I}_j)$ are not counted separately, we see that there are 15 different operators for H^{t}_{ss} given in Table X, 15 for H^{f}_{ss} given in Table XI, and 27 different operators for H^{tf}_{ss} given in Table XII. As in Ref. (*25*), it is convenient to try to reduce the large number of adjustable parameters associated with a general expression containing these operators by considering only that linear combination occurring in the classical dipole–dipole (spin–spin) interaction energy expression.

Consider first the classical expression W^{t}_{ss} describing nuclear spin–spin interaction wholly within the top. If top-fixed (t) vector components are used, this operator takes the form

$$W^{\mathrm{t}}_{ss} = g_{\mathrm{t}}^2\mu_{\mathrm{N}}^2 r_{\mathrm{t}}^{-3}[\mathbf{I}_1\cdot\mathbf{I}_2 - 3r_{\mathrm{t}}^{-2}(\mathbf{I}_1\cdot\mathbf{r}_{12})(\mathbf{r}_{12}\cdot\mathbf{I}_2) + \mathbf{I}_2\cdot\mathbf{I}_3 - 3r_{\mathrm{t}}^{-2}(\mathbf{I}_2\cdot\mathbf{r}_{23})(\mathbf{r}_{23}\cdot\mathbf{I}_3) + \mathbf{I}_3\cdot\mathbf{I}_1 - 3r_{\mathrm{t}}^{-2}(\mathbf{I}_3\cdot\mathbf{r}_{31})(\mathbf{r}_{31}\cdot\mathbf{I}_1)]_{\mathrm{t}}, \quad (34)$$

where g_{t} is the nuclear g-factor for the protons in the top, μ_{N} is the nuclear magneton, r_{t} is the distance between protons in the top, $\mathbf{r}_{ij} \equiv \mathbf{r}_i - \mathbf{r}_j$ are vectors from atom j to atom i, and the final subscript t indicates components taken in the top-fixed axis system.

Using standard procedures it is possible to express Eq. (34) in a relatively compact spherical tensor notation (*29–32*),

$$W^{\mathrm{t}}_{ss} = -3g_{\mathrm{t}}^2\mu_{\mathrm{N}}^2 r_{\mathrm{t}}^{-5}\sum_{ij}{}' \sum_{s} (-1)^s [T_{rijrij}(2, -s)T_{IiIj}(2, +s)]_{\mathrm{t}}, \quad (35)$$

where $\sum'$ indicates that j takes the values 2, 3, 1 when i takes the values 1, 2, 3, respectively. The index s takes the usual values ± 2, ± 1, 0. There are a variety of sign conventions in the literature for spherical tensors. We follow Edmonds (*29*) and relate spherical tensor components to Cartesian tensor components for two vector operators $\mathbf{r}_a$ and $\mathbf{r}_b$ by the equations

$$\begin{aligned} T_{rarb}(2, \pm 2) &= +(1/2)(x_a \pm iy_a)(x_b \pm iy_b) \\ T_{rarb}(2, \pm 1) &= \mp(1/2)[(x_a \pm iy_a)z_b + z_a(x_b \pm iy_b)] \\ T_{rarb}(2, 0) &= +6^{-1/2}(3z_a z_b - \mathbf{r}_a\cdot\mathbf{r}_b). \end{aligned} \quad (36)$$

Top-fixed components are used in Eq. (34) because the $\mathbf{r}_{ij}$ for $i, j = 1, 2, 3$ are all constants in the top-fixed axis system, with values determinable from Table I:

$$\begin{aligned} \mathbf{r}_{12}/r_{\mathrm{t}} &= +(\sqrt{3}/2)\mathbf{i} + (1/2)\mathbf{j} \\ \mathbf{r}_{23}/r_{\mathrm{t}} &= -\mathbf{j} \\ \mathbf{r}_{31}/r_{\mathrm{t}} &= -(\sqrt{3}/2)\mathbf{i} + (1/2)\mathbf{j}. \end{aligned} \quad (37)$$

Components of the tensors T_{rijrij} occurring in Eq. (35) are therefore also constants,

$$\begin{aligned} T_{rijrij}(2, \pm 2)_{\mathrm{t}} &= -(1/2)\omega^{\pm(2-i-j)}r_{\mathrm{t}}^2 \\ T_{rijrij}(2, \pm 1)_{\mathrm{t}} &= 0 \\ T_{rijrij}(2, 0)_{\mathrm{t}} &= -6^{-1/2}r_{\mathrm{t}}^2, \end{aligned} \quad (38)$$

where we define a quantity ω,

$$\omega \equiv e^{+2\pi i/3}, \tag{39}$$

which reflects the threefold symmetry in the molecule and which we shall make extensive use of in the derivations below.

We now convert the nuclear-spin tensor $T_{Ii Ij}$ in Eq. (35) from operators referring to the spins $\mathbf{I}_i$ and $\mathbf{I}_j$ of individual nuclei to the more "symmetrized" operators of Eqs. (24). The latter equations can be rewritten in terms of the quantity ω defined above as

$$\begin{aligned}(\mathbf{I}^{\mathrm{t}})_q &= \sqrt{3} \sum_n U_{qn}\mathbf{I}_n \\ (\mathbf{I}^{\mathrm{f}})_q &= \sqrt{3} \sum_n U_{qn}\mathbf{I}_{n+3} \\ U_{qn} &\equiv (1/\sqrt{3})\omega^{+q(n-1)},\end{aligned} \tag{40}$$

where the matrix U is unitary, and q and n both take on the values 1, 2, 3. Note that $q = 1, 2, 3$ in Eqs. (40) corresponds to $q = +1, -1, 0$ mod 3, and the notation of Eqs. (40) is thus consistent with the notation $q = +, -, 0$ used in Eqs. (24) and Tables VIII–XII. Substituting Eqs. (38) and the inverse transformation of the first of Eqs. (40) into Eq. (35) leads to an expression of the form

$$\begin{aligned}W^{\mathrm{t}}_{ss} = -g_{\mathrm{t}}^2\mu_{\mathrm{N}}^2 r_{\mathrm{t}}^{-3} \sum_{q,q'} \{ &[3^{-1} \sum_{ij}{}' \omega^{-q(i-1)-q'(j-1)-2+i+j}](-1/2)T_{qq'}(2, +2) \\ &+ [3^{-1} \sum_{ij}{}' \omega^{-q(i-1)-q'(j-1)}](-1/\sqrt{6})T_{qq'}(2, 0) \\ &+ [3^{-1} \sum_{ij}{}' \omega^{-q(i-1)-q'(j-1)+2-i-j}](-1/2)T_{qq'}(2, -2)\}_{\mathrm{t}}.\end{aligned} \tag{41}$$

It can be seen that $\sum'_{ij}$ in Eq. (41) is equivalent to $\sum_i$ with $i = 1, 2, 3$ and $j = i + 1$. Carrying out these operations yields

$$\begin{aligned}W^{\mathrm{t}}_{ss} = -g_{\mathrm{t}}^2\mu_{\mathrm{N}}^2 r_{\mathrm{t}}^{-3} \sum_{qq'} \{ &(\delta_{q',2-q})\omega^{q-1}(-1/2)T_{qq'}(2, +2) \\ &+ (\delta_{q',3-q})\omega^{q}(-1/\sqrt{6})T_{qq'}(2, 0) + (\delta_{q',4-q})\omega^{q+1}(-1/2)T_{qq'}(2, -2)\}_{\mathrm{t}},\end{aligned} \tag{42}$$

where q and q' take on the values 1, 2, 3 and the δ functions only require equality of their arguments *modulo* 3. Equations (36) and (42) show that the six operators in rows 6–8 of Table X are not present in the classical operator for spin–spin interaction within the top. (We note in passing that slightly different forms for Eq. (42) are obtained if we set $j = i + 1$, or $i = j + 1$, or use an average of the two. The Hamiltonians analogous to Eq. (34) corresponding to these three possibilities are all equal, however, so that no changes in the final results arise, *as long as one consistent choice is maintained.*)

We next convert the nuclear-spin operators from top-fixed (t) components to laboratory-fixed (L) components, since nuclear-spin basis functions are normally chosen to be characterized by laboratory-fixed projection quantum numbers. It is convenient,

however, to pass from (t) to (L) through the intermediate stage of molecule-fixed (M) components. Equations (23) indicate that the second-rank spherical tensor components defined in Eqs. (36) transform as follows,

$$T(2, s)_t = e^{+is\alpha p/m} e^{-is\alpha} T(2, s)_M$$

$$T(2, s)_f = e^{+is\alpha p/m} T(2, s)_M, \tag{43}$$

so that conversion from top- or frame-fixed components to molecule-fixed components is relatively easy.

It is convenient to change from molecule-fixed to laboratory-fixed Cartesian components of the nuclear-spin angular momentum operators in the products of interest using the relation

$$(I_M)_{q;\beta}(I_M)_{q';\beta'} = \sum_{B,B'} S_{\beta B} S_{\beta' B'} (I_L)_{q;B} (I_L)_{q';B'}, \tag{44}$$

where $S_{\beta B}$ represents the direction cosine matrix in the first of Eqs. (23) and is thus not a function of α. Since we restrict our attention to $\Delta J = 0$ hyperfine interactions in this paper, we desire an operator equivalent for $S_{\beta B} S_{\beta' B'}$ analogous to the operator equivalent $(J_L)_B (J_M)_\beta / J(J+1)$ used for $S_{\beta B}$ in Eq. (27). Because the nuclear-spin operators occurring in the spin–spin interaction Hamiltonian can be written as components of a symmetric traceless tensor, it is sufficient to use an operator equivalent for $\Delta J = 0$ from Eq. (3) of Ref. (*33*):

$$\begin{aligned}(1/2)[S_{\beta B} S_{\beta' B'} + S_{\beta B'} S_{\beta' B}] - (1/3)\delta_{\beta\beta'}\delta_{BB'} \rightarrow [6/J(J+1)(2J-1)(2J+3)] \\ \times [(1/2)(J_B J_{B'} + J_{B'} J_B) - (1/3)\delta_{BB'}\mathbf{J}^2] \\ \times [(1/2)(J_\beta J_{\beta'} + J_{\beta'} J_\beta) - (1/3)\delta_{\beta\beta'}\mathbf{J}^2].\end{aligned} \tag{45}$$

For $\Delta J = \pm 1$ and ± 2 matrix elements, more complicated ladder operator methods (*23*), or spherical tensor techniques (*29–32*) applied directly to Eq. (44), prove convenient. In the present case we apply the spherical tensor definitions of Eqs. (36) to Eq. (44) after substitution of Eq. (45) and obtain

$$\begin{aligned}T_{qq'}(2, \pm 2)_M &= [J_\pm^2]_M [3/J(J+1)(2J-1)(2J+3)] \\ &\quad \times [\sum_s (-1)^s T_{rot}(2, +s) T_{qq'}(2, -s)]_L \\ T_{qq'}(2, \pm 1)_M &= \mp [J_\pm J_z + J_z J_\pm]_M [3/J(J+1)(2J-1)(2J+3)] \\ &\quad \times [\sum_s (-1)^s T_{rot}(2, +s) T_{qq'}(2, -s)]_L \\ T_{qq'}(2, 0)_M &= \sqrt{6}[J_z^2 - (1/3)\mathbf{J}^2]_M [3/J(J+1)(2J-1)(2J+3)] \\ &\quad \times [\sum_s (-1)^s T_{rot}(2, +s) T_{qq'}(2, -s)]_L,\end{aligned} \tag{46}$$

where $T_{rot}(2, s)_L$ is a second-rank tensor constructed from laboratory-fixed components of the total angular momentum **J** according to Eqs. (36).

Substituting Eqs. (46) and the first of Eqs. (43) into Eq. (42), summing over q and q', and making use of the fact that $T_{qq'}(2, s) = T_{q'q}(2, s)$ for the nuclear-spin operators in Eqs. (40), we obtain finally for the classical spin–spin interaction energy within the top

$$W_{ss}^{t} = g_t^2 \mu_N^2 r_t^{-3} [3/J(J+1)(2J-1)(2J+3)] \sum_s (-1)^s T_{\rm rot}(2, +s)_L$$
$$\times \{(1/2)[J_+^2]_M e^{+2i\alpha p/m} e^{-2i\alpha} [T_{++}(2, -s)_L - T_{0-}(2, -s)_L]$$
$$+ [J_z^2 - (1/3)\mathbf{J}^2]_M [T_{00}(2, -s)_L - T_{+-}(2, -s)_L]$$
$$+ (1/2)[J_-^2]_M e^{-2i\alpha p/m} e^{+2i\alpha} [T_{--}(2, -s)_L - T_{0+}(2, -s)_L]\}, \quad (47)$$

where the +, −, 0 subscripts on the nuclear-spin operators $T_{qq'}$ match those in Eqs. (24), (25) and Tables VIII–XII, e.g.,

$$T_{0-}(2, 2)_L = (1/2)[(I_L^t)_{0;X} + i(I_L^t)_{0;Y})]\,[(I_L^t)_{-;X} + i(I_L^t)_{-;Y}]. \quad (48)$$

An analogous procedure can obviously be carried out for the classical spin–spin interaction energy W_{ss}^{f} within the frame,

$$W_{ss}^{f} = g_f^2 \mu_N^2 r_f^{-3} [\mathbf{I}_4 \cdot \mathbf{I}_5 - 3r_f^{-2}(\mathbf{I}_4 \cdot \mathbf{r}_{45})(\mathbf{r}_{45} \cdot \mathbf{I}_5)$$
$$+ \mathbf{I}_5 \cdot \mathbf{I}_6 - 3r_f^{-2}(\mathbf{I}_5 \cdot \mathbf{r}_{56})(\mathbf{r}_{56} \cdot \mathbf{I}_6) + \mathbf{I}_6 \cdot \mathbf{I}_4 - 3r_f^{-2}(\mathbf{I}_6 \cdot \mathbf{r}_{64})(\mathbf{r}_{64} \cdot \mathbf{I}_4)]_f, \quad (49)$$

except that here it is convenient to use frame-fixed (f) vector components so that the $\mathbf{r}_{ij}$ are again constants,

$$\mathbf{r}_{45}/r_f = +(\sqrt{3}/2)\mathbf{i} - (1/2)\mathbf{j}$$
$$\mathbf{r}_{56}/r_f = +\mathbf{j}$$
$$\mathbf{r}_{64}/r_f = -(\sqrt{3}/2)\mathbf{i} - (1/2)\mathbf{j}, \quad (50)$$

where r_f is now the proton–proton distance in the frame. The analog of Eq. (47) for W_{ss}^{f} becomes

$$W_{ss}^{f} = g_f^2 \mu_N^2 r_f^{-3} [3/J(J+1)(2J-1)(2J+3)] \sum_s (-1)^s T_{\rm rot}(2, +s)_L$$
$$\times \{(1/2)[J_+^2]_M e^{+2i\alpha p/m} [T_{--}(2, -s)_L - T_{0+}(2, -s)_L]$$
$$+ [J_z^2 - (1/3)\mathbf{J}^2]_M [T_{00}(2, -s)_L - T_{+-}(2, -s)_L]$$
$$+ (1/2)[J_-^2]_M e^{-2i\alpha p/m} [T_{++}(2, -s)_L - T_{0-}(2, -s)_L]\}. \quad (51)$$

When the analog of Eq. (42) for W_{ss}^{f} is written, using frame-fixed components for the nuclear-spin operators, it is seen that the six operators from rows 6–8 in Table XI do not occur in W_{ss}^{f}.

The classical energy expression W_{ss}^{tf} for nuclear-spin–spin interactions between the top and frame,

$$W_{ss}^{tf} = + g_t g_f \mu_N^2 r_{14}^{-3} [\mathbf{I}_1 \cdot \mathbf{I}_4 - 3r_{14}^{-2}(\mathbf{I}_1 \cdot \mathbf{r}_{14})(\mathbf{r}_{14} \cdot \mathbf{I}_4)$$
$$+ \mathbf{I}_2 \cdot \mathbf{I}_6 - 3r_{14}^{-2}(\mathbf{I}_2 \cdot \mathbf{r}_{26})(\mathbf{r}_{26} \cdot \mathbf{I}_6) + \mathbf{I}_3 \cdot \mathbf{I}_5 - 3r_{14}^{-2}(\mathbf{I}_3 \cdot \mathbf{r}_{35})(\mathbf{r}_{35} \cdot \mathbf{I}_5)]$$

$$+ g_t g_f \mu_N^2 r_{15}^{-3}[\mathbf{I}_1 \cdot \mathbf{I}_5 - 3r_{15}^{-2}(\mathbf{I}_1 \cdot \mathbf{r}_{15})(\mathbf{r}_{15} \cdot \mathbf{I}_5)$$

$$+ \mathbf{I}_2 \cdot \mathbf{I}_4 - 3r_{15}^{-2}(\mathbf{I}_2 \cdot \mathbf{r}_{24})(\mathbf{r}_{24} \cdot \mathbf{I}_4) + \mathbf{I}_3 \cdot \mathbf{I}_6 - 3r_{15}^{-2}(\mathbf{I}_3 \cdot \mathbf{r}_{36})(\mathbf{r}_{36} \cdot \mathbf{I}_6)]$$

$$+ g_t g_f \mu_N^2 r_{16}^{-3}[\mathbf{I}_1 \cdot \mathbf{I}_6 - 3r_{16}^{-2}(\mathbf{I}_1 \cdot \mathbf{r}_{16})(\mathbf{r}_{16} \cdot \mathbf{I}_6)$$

$$+ \mathbf{I}_2 \cdot \mathbf{I}_5 - 3r_{16}^{-2}(\mathbf{I}_2 \cdot \mathbf{r}_{25})(\mathbf{r}_{25} \cdot \mathbf{I}_5) + \mathbf{I}_3 \cdot \mathbf{I}_4 - 3r_{16}^{-2}(\mathbf{I}_3 \cdot \mathbf{r}_{34})(\mathbf{r}_{34} \cdot \mathbf{I}_4)], \quad (52)$$

is considerably more complicated to treat than W_{ss}^{t} or W_{ss}^{f}, since there is no possible choice of coordinate system in which all proton–proton distances $\mathbf{r}_{ij}$ remain constant. In what follows, we shall arbitrarily choose to examine W_{ss}^{tf} in detail in a frame-fixed axis system.

We first write the analog of Eq. (35) as

$$W_{ss}^{tf} = -3 g_t g_f \mu_N^2 \sum_s (-1)^s \sum_{ij} r_{ij}^{-5}[T_{rijrij}(2, -s) T_{IiIj}(2, +s)]_f, \quad (53)$$

where $i = 1, 2, 3$, $j = 4, 5, 6$, $s = \pm 2, \pm 1, 0$, and the final subscript f indicates components taken in the frame-fixed axis system.

We consider next the proton–proton vectors $\mathbf{r}_{ij}$. Since the first subscript $i = 1, 2, 3$ is always chosen from the top, and the second $j = 4, 5, 6$ is always chosen from the frame, and since frame-fixed vector components are used, we can write

$$[\mathbf{r}_{ij}]_f = S^{-1}(\alpha, 0, 0) \cdot [\mathbf{a}_i^0]_t - [\mathbf{a}_j^0]_f, \quad (54)$$

where components of the vectors $[\mathbf{a}_i^0]_t$ and $[\mathbf{a}_j^0]_f$ are given in Table I. Equation (54) leads immediately to various useful relations between the quantities $\mathbf{r}_{ij}$. For the squares of the distances occurring in Eq. (53) we find

$$\mathbf{r}_{14}^2(\alpha) = \mathbf{r}_{26}^2(\alpha) = \mathbf{r}_{35}^2(\alpha) = (\mathbf{a}_1^0)^2 + (\mathbf{a}_4^0)^2 - 2(a_{1z}^0)(a_{4z}^0) - 2(a_{1x}^0)(a_{4x}^0)\cos\alpha$$

$$\mathbf{r}_{15}^2(\alpha) = \mathbf{r}_{24}^2(\alpha) = \mathbf{r}_{36}^2(\alpha) = \mathbf{r}_{14}^2(\alpha - 2\pi/3)$$

$$= (\mathbf{a}_1^0)^2 + (\mathbf{a}_4^0)^2 - 2(a_{1z}^0)(a_{4z}^0) - 2(a_{1x}^0)(a_{4x}^0)\cos(\alpha - 2\pi/3)$$

$$\mathbf{r}_{16}^2(\alpha) = \mathbf{r}_{25}^2(\alpha) = \mathbf{r}_{34}^2(\alpha) = \mathbf{r}_{14}^2(\alpha + 2\pi/3)$$

$$= (\mathbf{a}_1^0)^2 + (\mathbf{a}_4^0)^2 - 2(a_{1z}^0)(a_{4z}^0) - 2(a_{1x}^0)(a_{4x}^0)\cos(\alpha + 2\pi/3). \quad (55)$$

For the tensors T_{rijrij} occurring in Eq. (53) we find

$$T_{r14r14}(2, s)_f = \omega^{+s} T_{r26r26}(2, s)_f = \omega^{-s} T_{r35r35}(2, s)_f$$

$$T_{r15r15}(2, s)_f = \omega^{+s} T_{r24r24}(2, s)_f = \omega^{-s} T_{r36r36}(2, s)_f$$

$$T_{r16r16}(2, s)_f = \omega^{+s} T_{r25r25}(2, s)_f = \omega^{-s} T_{r34r34}(2, s)_f. \quad (56)$$

Substituting Eqs. (55) and (56) in Eq. (53) after using Eqs. (40), we arrive at the analog of Eq. (42),

$$W_{ss}^{tf} = -g_t g_f \mu_N^2 \sum_s (-1)^s \sum_{qq'} \delta_{q',q-s}\{[r_{14}^{-5} T_{r14r14}(2, -s)$$

$$+ \omega^{s-q} r_{15}^{-5} T_{r15r15}(2, -s) + \omega^{q-s} r_{16}^{-5} T_{r16r16}(2, -s)] T_{qq'}(2, +s)\}_f, \quad (57)$$

where $q, q' = 1, 2, 3$, and the δ function only requires equality of its arguments *modulo* 3. Equation (57) differs slightly from Eq. (42) in that the components of the tensors T_{rijrij} have not yet been explicitly evaluated. Equations (36) and (57) show that all operators from Table XII are present in W_{ss}^{tf}.

The conversion from frame-fixed components to laboratory-fixed components for the nuclear-spin tensors $T_{qq'}$ in Eq. (57) can be carried out using the second of Eqs. (43), and then Eqs. (46), to yield

$$W_{ss}^{tf} = -g_t g_f \mu_N^2 [6/J(J+1)(2J-1)(2J+3)] \sum_s (-1)^s e^{+is\alpha p/m}$$
$$\times T_{rot}(2, +s)_M \sum_{qq'} \delta_{q',q-s} [r_{14}^{-5} T_{r14r14}(2, -s) + \omega^{s-q} r_{15}^{-5} T_{r15r15}(2, -s)$$
$$+ \omega^{q-s} r_{16}^{-5} T_{r16r16}(2, -s)]_f \sum_r (-1)^r [T_{rot}(2, +r) T_{qq'}(2, -r)]_L, \quad (58)$$

where Eq. (58) is applicable only for $\Delta J = 0$ matrix elements, and where the spherical tensors $T_{rot}(2, s)_M$ involving the molecule-fixed components of the angular momentum are best evaluated after converting to normal ladder operators (using Eqs. (36)), to avoid difficulties arising from the anomalous sign of i in the commutation relations of the components of $[\mathbf{J}]_M$.

The tensors T_{r1jr1j} in Eq. (58) can be evaluated for $j = 4, 5, 6$ from Eqs. (36) and (54).

$$T_{r1jr1j}(2, \pm 2) = (1/2)[e^{\pm i\alpha}(a_{1x}^0) - \omega^{\pm(j-4)}(a_{4x}^0)]^2$$
$$= (1/2)[e^{\pm 2i\alpha}(a_{1x}^0)^2 - 2\omega^{\pm(j-4)} e^{\pm i\alpha}(a_{1x}^0)(a_{4x}^0) + \omega^{\pm(4-j)}(a_{4x}^0)^2]$$
$$T_{r1jr1j}(2, \pm 1) = \mp[e^{\pm i\alpha}(a_{1x}^0) - \omega^{\pm(j-4)}(a_{4x}^0)][(a_{1z}^0) - (a_{4z}^0)]$$
$$T_{r1jr1j}(2, 0) = \sqrt{6}(1/2)[(a_{1z}^0 - a_{4z}^0)^2 - (1/3) r_{1j}^2], \quad (59)$$

where we have made use of the fact that $z_{14} = z_{15} = z_{16}$. Substitution of Eqs. (59) in Eq. (58) yields the final expression for W_{ss}^{tf}.

4. APPLICATION TO EXPERIMENTAL DATA

In this section we use the hyperfine interaction formalism derived in the previous section to discuss various observed and unobserved anticrossings from the molecular beam investigations. The avoided crossings of interest here fall into two categories which, in the language of Refs. (*5–8*), are called "barrier" anticrossings when $\Delta|K| = 0$ and "hyperfine" anticrossings when $\Delta|K| = 1$ or 2. In both cases it is hyperfine matrix elements off-diagonal in the vibration–rotation–torsion symmetries of the wavefunctions that provide the coupling between the anticrossing levels. We first discuss the calculation of matrix elements in general and then discuss in some detail the CH_3SiH_3 (*5*) and CH_3SiF_3 (*6*) molecules, since they have been subjected to the most thorough experimental study.

A. Matrix Elements of the Nuclear Spin–Spin Operators

The wavefunctions in Table XIII are written in the high-field representation appropriate (*3*) to the anticrossing experiments. The levels are characterized by the

quantum numbers (J, K, σ, m_J, I_t, M_t, I_f, M_f). A relatively strong electric field is applied in order to bring the levels involved to their avoided crossing. The wavefunctions in Table XIII do not belong to one of the $^{trn}\Gamma$ species A_1 or A_2 allowed by the Pauli exclusion principle for the group G_{18}. In zero external field these A_1 and A_2 wavefunctions occur in nearly degenerate pairs, and each such pair is fully mixed by the strong Stark effect to generate a sum and difference function. It is these 50:50 mixtures which are listed in Table XIII. The levels with $K = \sigma = 0$ are exceptions; in this case the symmetry is A_1 or A_2.

A small magnetic field ($\sim$2 mT) is assumed for two reasons. First, it is possible (*3*) to have two distinct levels which are degenerate with respect to the Stark energy but which can be coupled by the nuclear hyperfine interactions. For these special cases, the representation in Table XIII breaks down in zero magnetic field. Fortunately, in almost all these cases the Zeeman energy lifts the degeneracy and simplifies the analysis. Second, the treatment of the avoided crossings generally assumes that the transitions occur within a series of separate two-level systems. In zero magnetic field, multilevel systems can arise, such as those in the Stark-hyperfine hybrids discussed in Ref. (*3*). In almost all of these special cases, the Zeeman energy reduces the multilevel systems to two-level problems and so simplifies the analysis. The Zeeman splitting is of particular importance because the special cases which can arise when $|K| = |m_J| = 1$

TABLE XIII

Complete Torsion–Rotation–Nuclear-Spin Wavefunctions for the States of H_3C–SiH_3 Shown in Fig. 2 of Ref. (*5*) and the States of H_3C–SiF_3 Shown in Fig. 2 of Ref. (*6*)

$\|J\ K\ \sigma\ \Gamma\ m_J\rangle$	$\|^t\Gamma\rangle\|^r\Gamma;J,K,M_J\rangle\|^{nt}\Gamma;I_t,M_t\rangle\|^{nf}\Gamma;I_f,M_f\rangle$[c]
$\|1,\pm1,\mp1,E_3,\pm1\rangle$[a]	$\|^tE_{m+p,0\mp}\rangle\|^rE_{p1\pm};1,\pm1,\pm1\rangle\|^{nt}E_{m1\pm};1/2,M_t\rangle\|^{nf}E_{01\pm};1/2,M_f\rangle$
$\|1,\mp1,\mp1,E_2,\pm1\rangle$[a]	$\|^tE_{m-p,0\mp}\rangle\|^rE_{p1\mp};1,\mp1,\pm1\rangle\|^{nt}E_{m1\pm};1/2,M_t\rangle\|^{nf}A_1;3/2,M_f\rangle$
$\|1,\mp1,\mp1,E_2,\mp1\rangle$[a]	$\|^tE_{m-p,0\mp}\rangle\|^rE_{p1\mp};1,\mp1,\mp1\rangle\|^{nt}E_{m1\pm};1/2,M_t\rangle\|^{nf}A_1;3/2,M_f\rangle$
$\|1,\mp1,0,E_1,\pm1\rangle$[a]	$\|^tE_{p0\pm}\rangle\|^rE_{p1\mp};1,\mp1,\pm1\rangle\|^{nt}A_1;3/2,M_t\rangle\|^{nf}E_{01\pm};1/2,M_f\rangle$
$\|2,\pm2,\mp1,E_2,\pm2\rangle$[b]	$\|^tE_{m+2p,0\mp}\rangle\|^rE_{2p,2\pm};2,\pm2,\pm2\rangle\|^{nt}E_{m1\pm};1/2,M_t\rangle\|^{nf}A_1;3/2,M_f\rangle$
$\|2,\pm2,\pm1,E_3,\pm2\rangle$[b]	$\|^tE_{m-2p,0\pm}\rangle\|^rE_{2p,2\pm};2,\pm2,\pm2\rangle\|^{nt}E_{m1\mp};1/2,M_t\rangle\|^{nf}E_{01\mp};1/2,M_f\rangle$
$\|2,\pm2,0,E_1,\pm2\rangle$[b]	$\|^tE_{2p,0\mp}\rangle\|^rE_{2p,2\pm};2,\pm2,\pm2\rangle\|^{nt}A_1;3/2,M_t\rangle\|^{nf}E_{01\pm};1/2,M_f\rangle$
$\|2,0,\pm1,E_4,0\rangle$[b]	$\|^tE_{m,0\pm}\rangle\|^rA_1;2,0,0\rangle\|^{nt}E_{m1\mp};1/2,M_t\rangle\|^{nf}E_{01\pm};1/2,M_f\rangle$
$\|2,0,0,A_1,0\rangle$[b]	$\|^tA_1\rangle\|^rA_1;2,0,0\rangle\|^{nt}A_1;3/2,M_t\rangle\|^{nf}A_1;3/2,M_f\rangle$

[a] In the notation of Fig. 2 and Table I of Ref. (5). Note that these wave functions in Ref. (5) do not contain nuclear spin factors, and that Γ corresponds to the torsion-rotation symmetry species.

[b] In the notation of Fig. 2 and Table 2 of Ref. (6). Note that these wave functions in Ref. (6) do not contain nuclear spin factors, and that Γ corresponds to the torsion-rotation symmetry species.

[c] In the notation of the present paper. The left superscripts t, r, nt and nf indicate IAM torsional and rotational functions, and laboratory-fixed nuclear spin functions for the top and frame nuclei, respectively. I_t and I_f represent the total spin angular momentum of the top and frame, respectively. Note that the same nuclear spin functions use here are suitable for use with the torsion-rotation wavefunctions defined in Refs. (5) and (6).

have been studied experimentally. For the fields assumed here, the Zeeman energy is much smaller in magnitude than the Stark energy, so that the 50:50 $A_1 + A_2$ mixtures in Table XIII still form an appropriate basis.

Matrix elements of various operators in the basis set of Table XIII can conveniently be separated into a torsional factor, a rotational factor, and a nuclear-spin factor, which we now comment on in turn.

The torsional factors were evaluated numerically, using a previously written computer program. The torsional wavefunctions used were obtained for each (σ, K) pair by diagonalizing the zeroth-order Hamiltonian matrix (*5*) set up in the IAM free rotor basis (*5*). The non-totally-symmetric part of a given exponential function of α in Eqs. (47), (51), and (58) is required to give nonzero matrix elements between torsional functions of different symmetry species.

Because the molecules considered here all have relatively high barriers, it is also of interest to calculate the torsional factor algebraically, using the high-barrier torsional wavefunction results from Ref. (*12*),

$$|E_{r0\pm}\rangle = (3m)^{-1/2} \sum_{k=0}^{3m-1} e^{\pm 2\pi i(k+1/2)r/3m} \psi_k(\alpha/m), \tag{60}$$

where $\psi_k(\alpha/m)$ is a torsional wavefunction localized in the kth minimum. These functions are like those shown in Fig. 4 of Ref. (*12*), except that for the present set of molecules, which have staggered equilibrium configurations, the minima occur at $(\alpha/m) = (k + 1/2)(2\pi/3m)$, rather than at $k(2\pi/3m)$ as in that figure, and each function $|E_{r0\pm}\rangle$ has thus, for convenience, been multiplied by an extra phase factor $e^{\pm\pi ir/3m}$. In the simplest approximation, one can (i) consider only nontunneling contributions to the torsional matrix element of a given operator (an approximation which may be expected to introduce fractional errors of the order of the tunneling splitting divided by the torsional frequency), and (ii) use a delta function for the ground state vibrational wave function localized in each minimum. If we use the high-barrier torsional functions of Eq. (60), and if further the delta function approximation is made, then the torsional integral can be obtained simply by evaluating the appropriate part of the integrand at one of the equilibrium configurations. For the molecular structures (*13, 34*) and barrier heights (*5, 6*) employed, values for a given matrix element evaluated by the two procedures differ by only a few percent.

In the rotational factor, the reduced matrix element for $T_{\rm rot}(2)_{\rm L}$ can easily be determined (*29*) to be

$$\langle J \| T_{\rm rot}(2) \| J \rangle = [(2J-1)2J(2J+1)(2J+2)(2J+3)/24]^{1/2}. \tag{61}$$

For the nuclear-spin tensors, the reduced matrix elements can also be determined by standard procedures. The tensors $T_{qq'}(2, s)_{\rm L}$ (for $s = -2, -1, 0, +1, +2$ and fixed q, q') occurring in Eq. (47) (i.e., in $W^{\rm t}_{ss}$) are constructed from products of laboratory-fixed components of the vectors $(\mathbf{I}^{\rm t}_{\rm L})_q$ and $(\mathbf{I}^{\rm t}_{\rm L})_{q'}$, and we find the following nonzero reduced matrix elements,

$$\langle {}^{\rm nt}A_1; 3/2 \| T_{0,0}(2) \| {}^{\rm nt}A_1; 3/2 \rangle = +(30)^{1/2}$$

$$\langle {}^{\rm nt}A_1; 3/2 \| T_{\pm,\mp}(2) \| {}^{\rm nt}A_1; 3/2 \rangle = -(30/4)^{1/2}$$

$$\langle {}^{\rm nt}A_1; 3/2 \| T_{\pm,\pm}(2) \| {}^{\rm nt}E_{m1\pm}; 1/2 \rangle = +(15)^{1/2}$$

$$\langle {}^{\mathrm{nt}}A_1;\, 3/2 \| T_{0,\pm}(2) \text{ or } T_{\pm,0}(2) \| {}^{\mathrm{nt}}E_{m1\mp};\, 1/2 \rangle = -(15/4)^{1/2}$$

$$\langle {}^{\mathrm{nt}}E_{m1\mp};\, 1/2 \| T_{\pm,\pm}(2) \| {}^{\mathrm{nt}}A_1;\, 3/2 \rangle = -(15)^{1/2}$$

$$\langle {}^{\mathrm{nt}}E_{m1\pm};\, 1/2 \| T_{0,\perp}(2) \text{ or } T_{\perp,0}(2) \| {}^{\mathrm{nt}}A_1;\, 3/2 \rangle = +(15/4)^{1/2}. \tag{62}$$

Similarly, the tensors $T_{qq'}(2, s)_{\mathrm{L}}$ occurring in Eq. (51) for W^{f}_{ss} are constructed from products of components of $(\mathbf{I}^{\mathrm{f}}_{\mathrm{L}})_q$ and $(\mathbf{I}^{\mathrm{f}}_{\mathrm{L}})_{q'}$, and we find nonzero reduced matrix elements given by Eqs. (62) with nt → nf and $E_{m1\pm} \rightarrow E_{01\mp}$.

The tensors $T_{qq'}(2, r)_{\mathrm{L}}$ occurring in Eq. (58) for W^{tf}_{ss} are constructed from products of components of $(\mathbf{I}^{\mathrm{t}}_{\mathrm{L}})_q$ and $(\mathbf{I}^{\mathrm{f}}_{\mathrm{L}})_{q'}$. Since in the basis set of Table XIII, nuclear spins in the top are not coupled to nuclear spins in the frame, it is necessary to express the second-rank tensor operators $T_{qq'}(2, +r)_{\mathrm{L}}$ in Eq. (58) in terms of first-rank tensors acting on *either* the spins in the top *or* the spins in the frame (see Eqs. (40)). Matrix elements of the tensor operators $T_{qq'}(2, r)_{\mathrm{L}}$ in Eq. (58) thus take the form (*29*)

$$\langle {}^{\mathrm{nt}}\Gamma';\, I'_{\mathrm{t}}M'_{\mathrm{t}} | \langle {}^{\mathrm{nf}}\Gamma';\, I'_{\mathrm{f}}M'_{\mathrm{f}} | T_{qq'}(2, r)_{\mathrm{L}} | {}^{\mathrm{nt}}\Gamma;\, I_{\mathrm{t}}M_{\mathrm{t}} \rangle | {}^{\mathrm{nf}}\Gamma;\, I_{\mathrm{f}}M_{\mathrm{f}} \rangle$$

$$= \sum_m (1, m, 1, r-m | 1, 1, 2, r) \langle {}^{\mathrm{nt}}\Gamma';\, I'_{\mathrm{t}}M'_{\mathrm{t}} | T_{\mathrm{q}}(1, m)_{\mathrm{L}} | {}^{\mathrm{nt}}\Gamma;\, I_{\mathrm{t}}M_{\mathrm{t}} \rangle$$

$$\times \langle {}^{\mathrm{nf}}\Gamma';\, I'_{\mathrm{f}}M'_{\mathrm{f}} | T_{q'}(1, r-m)_{\mathrm{L}} | {}^{\mathrm{nf}}\Gamma;\, I_{\mathrm{f}}M_{\mathrm{f}} \rangle, \tag{63}$$

where the operator $T_q(1, m)$ in the first matrix element on the right of Eq. (63) contains only nuclear-spin operators for atoms in the top and the operator $T_{q'}(1, r - m)$ in the second matrix element contains only spin operators for atoms in the frame. Phase factors for spherical tensors of rank 1 (*29*) can be defined by an analog of Eqs. (36),

$$T_{\mathrm{r}}(1, \pm 1) = \mp(1/\sqrt{2})(x \pm iy)$$

$$T_{\mathrm{r}}(1, 0) = z. \tag{64}$$

Nonvanishing reduced matrix elements of the first-rank tensors required to evaluate Eq. (63) when operators and wavefunctions apply to the top are then as follows,

$$\langle {}^{\mathrm{nt}}\Gamma;\, I \| T_0(1) \| {}^{\mathrm{nt}}\Gamma;\, I \rangle = +[I(I+1)(2I+1)]^{1/2}$$

$$\langle {}^{\mathrm{nt}}A_1;\, 3/2 \| T_{\pm}(1) \| {}^{\mathrm{nt}}E_{m1\mp};\, 1/2 \rangle = -\sqrt{6}$$

$$\langle {}^{\mathrm{nt}}E_{m1\pm};\, 1/2 \| T_{\pm}(1) \| {}^{\mathrm{nt}}A_1;\, 3/2 \rangle = +\sqrt{6}$$

$$\langle {}^{\mathrm{nt}}E_{m1\mp};\, 1/2 \| T_{\pm}(1) \| {}^{\mathrm{nt}}E_{m1\pm};\, 1/2 \rangle = -\sqrt{6}. \tag{65}$$

Nonvanishing reduced matrix elements required when operators and wavefunctions apply to the frame are given by Eqs. (65) with nt → nf and $E_{m1\pm} \rightarrow E_{01\mp}$.

Because of various phase conventions, reduced matrix elements defined in connection with spherical tensors are often not Hermitian. Thus, since the spherical tensors defined in terms of **r** in Eqs. (36) and (64) satisfy Eq. (5.5.2) of Edmonds (*29*) when **r** is replaced by any of the operators considered in this paper, their reduced matrix elements in Eqs. (62) and (65) satisfy Eq. (5.5.4) of that reference, i.e.,

$$(\gamma' j' \| \mathbf{T}(k) \| \gamma j) = (-1)^{j'-j} (\gamma j \| \mathbf{T}^{\dagger}(k) \| \gamma' j')^*. \tag{66}$$

Matrix elements for nuclear-spin operators obtained using Eqs. (62) and (65) are,

however, consistent with matrix elements for the same operators obtained using the reduced matrix elements in Eqs. (53) of Ref. (*25*), which are defined there to be Hermitian, as is commonly done when using ladder operator techniques (*23, 25*).

Matrix elements H_{ss} of the operators in Eqs. (47), (51), and (58) can now be evaluated by standard spherical tensor procedures (*29*). Since the molecular geometries and nuclear magnetic dipole moments are known, there are no adjustable parameters in this evaluation. (The electron-coupled contribution is neglected.) Various matrix elements are collected in Table XIV. Twelve anticrossings have been selected that illustrate the anomaly discussed in Section 1. The first six are hyperfine anticrossings in CH_3SiF_3 with $K = \pm 2 \leftrightarrow 0$. Rows 7 through 9a refer to barrier anticrossings in CH_3SiH_3 with $K = \pm 1 \leftrightarrow \mp 1$. Rows 10 through 12a refer to a similar set of barrier anticrossings in CH_3SiF_3, but with $J = 2$ instead of $J = 1$.

In Table XIV, rotational and torsional quantum numbers for the two states participating in the avoided crossing are given in columns 2–6 and 7–11, respectively. Corresponding nuclear-spin projection quantum numbers for top and frame nuclei are

TABLE XIV

Matrix Elements[a] for Various Anticrossings

#[b]	J'	K'	σ'	Γ'	m_J'	J	K	σ	Γ	m_J	M_t'	M_f'	M_t	M_f	$\lvert H_{ss}\rvert$[c]		I_{calc}[d]	I_{obs}[e]
1	2	±2	0	E_1	±2	2	0	±1	E_4	0	∓3/2	M_f	±1/2	M_f	7.706	t	4.0000	4.7
1a	2	±2	0	E_1	±2	2	0	∓1	E_4	0	∓3/2	∓1/2	∓1/2	±1/2	0.497	tf	0.1112	U
2	2	±2	∓1	E_2	±2	2	0	∓1	E_4	0	M_t	∓3/2	M_t	±1/2	2.460	f	2.8932	2.4
2a	2	±2	∓1	E_2	±2	2	0	±1	E_4	0	∓1/2	∓3/2	±1/2	∓1/2	0.497	tf	0.1112	U
3	2	±2	±1	E_3	±2	2	0	±1	E_4	0	∓1/2	∓1/2	±1/2	±1/2	0.156	tf	0.0083	No
3a	2	±2	±1	E_3	±2	2	0	∓1	E_4	0	∓1/2	∓1/2	±1/2	±1/2	0.040	tf	0.0005	No
4	2	±2	∓1	E_2	±2	2	0	0	A_1	0	∓1/2	M_f	±3/2	M_f	7.706	t	8.0000	8.5
5	2	±2	0	E_1	±2	2	0	0	A_1	0	M_t	∓1/2	M_t	±3/2	2.460	f	5.7864	3.0
6	2	±2	±1	E_3	±2	2	0	0	A_1	0	±1/2	±1/2	±3/2	±3/2	0.431	tf	0.1120	No
7	1	±1	∓1	E_3	±1	1	∓1	0	E_1	±1	±1/2	M_f	±1/2	M_f	4.682	t	2.5740	2.70
7a	1	±1	∓1	E_3	±1	1	±1	0	E_1	∓1	±1/2	∓1/2	±3/2	±1/2	0.814	tf	0.0693	No
8	1	±1	∓1	E_3	±1	1	∓1	∓1	E_2	±1	M_t	±1/2	M_t	±1/2	1.920	f	0.5552	0.51
8a	1	±1	∓1	E_3	±1	1	±1	±1	E_2	∓1	∓1/2	±1/2	±1/2	±3/2	0.814	tf	0.0693	No
9	1	±1	±1	E_2	±1	1	∓1	0	E_1	±1	±1/2	±1/2	±1/2	±1/2	0.227	tf	0.0122	No
9a	1	±1	±1	E_2	±1	1	±1	0	E_1	∓1	±1/2	∓3/2	±3/2	∓1/2	0.705	tf	0.0695	No
10	2	±1	∓1	E_3	±1	2	∓1	0	E_1	±1	±1/2	M_f	±1/2	M_f	3.337	t	3.8553	Yes
10a	2	±1	∓1	E_3	±1	2	±1	0	E_1	∓1	±1/2	∓1/2	±3/2	±1/2	0.519	tf	0.1212	U
11	2	±1	∓1	E_3	±1	2	∓1	∓1	E_2	±1	M_t	±1/2	M_t	±1/2	1.065	f	0.7264	Yes
11a	2	±1	∓1	E_3	±1	2	±1	±1	E_2	∓1	∓1/2	±1/2	±1/2	±3/2	0.519	tf	0.1212	U
12	2	±1	±1	E_2	±1	2	∓1	0	E_1	±1	±1/2	±1/2	±1/2	±1/2	0.144	tf	0.0212	No
12a	2	±1	±1	E_2	±1	2	±1	0	E_1	∓1	±1/2	∓3/2	±3/2	∓1/2	0.450	tf	0.1220	No

[a] Rotational and torsional quantum numbers for the two states involved in the matrix element of a given row are given in columns 2-6 and 7-11 in the notation of Fig. 1 and Table I of Ref. (5). Laboratory-fixed top and frame nuclear spin projection quantum numbers are given in columns 12-15.

[b] Arbitrary number for convenient reference. Matrix elements in rows 1-6 are for CH_3SiF_3 and correspond to the avoided crossings shown in Fig. 2 of Ref. (6). Matrix elements in rows 7-9 are for CH_3SiH_3, and correspond to the avoided crossings shown in Fig. 2 of Ref. (5). Matrix elements in rows 10-12 are for CH_3SiF_3 (6). Quantum numbers indicated in rows 1a, 2a, etc. represent alternative Δm_J and/or $\Delta\sigma$ assignments for crossings in the corresponding rows 1, 2, etc.

[c] The symbol t (top), f (frame) or tf indicates a matrix element H_{ss} calculated from Eq. (47), (51) or (58), respectively.

[d] Fraction of the full intensity available, as calculated from Eq. (67).

[e] Observed (Yes), unobserved (No), and untested (U) lines, or arbitrarily normalized relative intensities within a group, if available.

given in columns 12–15. The label tf in the column headed $|H_{ss}|$ indicates rows where matrix elements of W^{t}_{ss} in Eq. (47) and W^{f}_{ss} in Eq. (51) are both zero for any choice of nuclear-spin projection quantum numbers M'_t, M'_f, M_t, M_f; for these rows nonzero contributions are only possible from W^{tf}_{ss} in Eq. (58). Furthermore, if several values for the nuclear-spin quantum numbers in these rows lead to nonzero matrix elements, only the set giving the matrix element of maximum absolute value is shown. The labels t or f in the column headed $|H_{ss}|$ indicate rows where contributions are possible from H^{t}_{ss} or H^{f}_{ss}, respectively, in addition to contributions from H^{tf}_{ss}. Since contributions from H^{tf}_{ss} turned out to be significantly smaller than those from H^{t}_{ss} or H^{f}_{ss}, only matrix elements for the latter two operators are given. For such matrix elements, either M_t or M_f does not change.

All rows but three in Table XIV are associated in pairs, corresponding to a simultaneous change in sign of the quantum numbers in the K, σ, and m_J columns. (The exceptions are rows 4, 5, 6, for which $K = \sigma = m_J = 0$.) For each of the pairs in rows 7 through 12, the two assignments correspond in a magnetic field to two distinct two-level problems. For each of the pairs in rows 1 through 3, there arise (for specific sets of the nuclear-spin quantum numbers) three-level systems which cannot be reduced to two-level problems by applying a magnetic field. However, for each such case in rows 1 and 2, the coupling between two of the three levels involved dominates. Thus, with the possible exception of some of the magnetic components in the pair (3, 3a), the transition probabilities of interest can be calculated using a suitable two-level model.

The large AC Stark effect associated with the permanent dipole moment of symmetric-top molecules introduces important modifications (*15*) in the standard two-level problem (*10*), so that when the avoided crossings are characterized by interaction matrix elements below a certain threshold, the maximum transition probability in a molecular beam electric resonance experiment drops below unity. For the CH_3SiF_3 measurements (*6*) considered here (6.2-cm-long C-field), unity transition probability can be achieved only when the energy separation $\nu_c = 2|H_{ss}|$ at the avoided crossing is greater than $\nu_{min} = 7.6$ kHz (*15*); for the CH_3SiH_3 measurements (*5*) (3.0-cm C-field), $\nu_{min} = 15.8$ kHz. If $\nu_c < \nu_{min}$, the maximum possible transition probability is given by (*15*)

$$\sin^2[(\nu_c/\nu_{min})(\pi/2)] = \sin^2[(H_{ss}/\nu_{min})\pi]. \tag{67}$$

Since the minimum energy separation at the avoided crossing is twice the interaction matrix element, we have replaced (ν_c/ν_{min}) by $2(H_{ss}/\nu_{min})$ on the right of Eq. (67), where H_{ss} represents any of the nuclear spin–spin matrix elements of Eq. (47), (51), or (58).

Column 17 of Table XIV gives a calculated value (I_{calc}) for the molecular beam electric resonance relative signal intensity. This value represents a sum of contributions, one from the hyperfine matrix element actually shown, plus others from hyperfine matrix elements characterized by other possible sets of nuclear-spin projection quantum numbers. For example, I_{calc} in row 1 is simply four times the value 1.0 obtained when $|H_{ss}| \geq 3.8$ kHz. The factor of 4 arises from the upper and lower sign choices indicated, and from the two additional choices of $M'_f = M_f = \pm\frac{1}{2}$. I_{calc} in row 5 is eight times the value obtained when $|H_{ss}| = 2.460$ is substituted into Eq. (67). The factor of 8

arises from the upper and lower signs indicated, and from the values of $M_t' = M_t = \pm\frac{1}{2}$ and $\pm\frac{3}{2}$. I_{calc} in row 1a involves twice the sum over two different $|H_{ss}|$ values, etc. Adding the intensities together implies an instrumental linewidth large enough to encompass any splittings caused by the small magnetic field mentioned earlier. For smaller instrumental linewidths and/or larger magnetic fields, the transitions in any given row may split into a number of resolvable components, though the details of such splittings depend on the nuclear-spin quantum numbers in the row and on the molecule involved. If the magnetic field and transition are such that only one two-level system in a given row falls within the instrumental linewidth, and indeed if this is the two-level system of maximum intensity in that row, then it is appropriate to discard the summed intensity entry in column 17, and to use instead the one-transition relative signal intensity obtained by substituting $|H_{ss}|$ from that row into Eq. (67).

B. Neglect of Nuclear Spin–Rotation Interaction

It is difficult to calculate the relative contributions of spin–rotation and spin–spin interactions to the matrix elements giving rise to the observed avoided crossings, because the magnitude of the relevant spin–rotation coupling constant cannot be estimated a priori to sufficient accuracy. However, arguments can be advanced which suggest that spin–rotation interaction can be neglected in the present discussion of observed and unobserved avoided crossings. For rows 1–6 in Table XIV, $\Delta m_J = \pm 2$. In general $|\Delta m_J| \leqslant 1$ for a spin–rotation term in the Hamiltonian matrix, so that only the spin–spin interaction can contribute to rows 1–6. For rows 7–12, an assignment with $\Delta m_J = 0$ is possible, and this argument does not apply. However, both for CH_3SiH_3 (*5*) and CH_3SiF_3 (*6*), it was found that anticrossings for which $3m_J^2 - J(J+1) = 0$ could not be detected, whereas corresponding anticrossings for which $3m_J^2 - J(J+1) \neq 0$ could be easily observed. Since spin–spin matrix elements vanish when $3m_J^2 = J(J+1)$, while spin–rotation matrix elements do not, this observation suggests strongly that spin–spin effects dominate spin–rotation effects when both are present (at least for the anticrossings which were detected). We thus confine attention in what follows to spin–spin interactions only.

C. Previous Observations in CH_3SiF_3 and CH_3SiH_3

The status, before the present work, of experimental observations with regard to the 12 anticrossings in Table XIV is specified in the last column of Table XIV. In this column an avoided crossing is characterized as observed (Yes), unobserved (No), untested (U), or by relative intensity information where available. Each U that occurs refers to an alternative assignment for an anticrossing characterized as observed. For these cases, the choice between U and Yes is based on the calculations presented here, rather than on magnetic field studies of the type discussed in Refs. (*5*), (*6*).

Figure 2 of Ref. (*6*) illustrates four observed (heavy dots) and two unobserved (no dots) "hyperfine" avoided crossings between $K = \pm 2$ and $K = 0$ levels for $J = 2$ in CH_3SiF_3. Because no magnetic studies were carried out for the anticrossing between $\Gamma' = E_2$ and $\Gamma = E_4$, the assignments given in rows 2 and 2a could not be distinguished at that time, and assignment 2a was selected in Fig. 2 and Table 2 of Ref. (*6*). In view

of the intensity calculations in Table XIV, we conclude that the earlier assignment should be changed to that in row 2.

It can be seen from the relative intensities given for the observed transitions in rows 1–6, that stronger lines correspond to larger values of I_{calc}, but that the ratio of observed to predicted values ranges from 0.5 to 1.2. These discrepancies between predicted and observed relative intensities presumably arise from the difficulties of making good intensity measurements, particularly since the spectra examined for Table XIV were originally recorded without any intention of determining accurate relative intensities. In addition, the effects of field inhomogeneities have not been taken into account. It is nevertheless satisfying to note that the unobserved avoided crossings are predicted theoretically to be considerably weaker than those actually observed.

Figure 2 of Ref. (*5*) illustrates two observed (heavy dots) and one unobserved (no dot) "barrier" avoided crossing for the $J = |K| = 1$ states of CH_3SiH_3. These crossings correspond to the matrix elements in rows 7–9 of Table XIV, and were chosen for discussion here because both careful magnetic studies and careful searches for the missing crossing were carried out.

In the Zeeman studies described in Refs. (*3, 5, 6*), the behavior of an avoided crossing when a magnetic field is applied allows one to distinguish between assignments with $\Delta m_J = \pm 2$ and those with $\Delta m_J = 0$. For these two types of anticrossings, the spectral lines are, respectively, split and unaffected by the Zeeman effect. Because the observed spectra were not "magnetically active," the $\Delta m_J = \pm 2$ assignments, corresponding to rows 7a and 8a, were experimentally rejected (*5*) in favor of the assignments in rows 7 and 8. From Table XIV we see that signals from the rejected mixing mechanisms are expected theoretically to be only 3% of the stronger observed signal.

Anticrossings of the type specified in rows 9 and 9a were the most puzzling in the selection rule studies carried out previously. For CH_3SiH_3 (*5*), CH_3SiF_3 (*6*), and CH_3CD_3 (*7, 8*), attempts were made to observe these $\Gamma' = E_2 \leftrightarrow \Gamma = E_1$ anticrossings for a variety of values of $J' = J$, m'_J, and m_J. Studies were carried out both with and without a magnetic field. None of these attempts was successful. These results were surprising because the $E_2 \leftrightarrow E_1$ anticrossings are so similar to those for $E_3 \leftrightarrow E_1$ (row 7) and $E_3 \leftrightarrow E_2$ (row 8), both of which were easily detected. On the one hand, it was tempting to attribute the difference in detectability to a smaller mixing matrix element; on the other hand, within the framework of the standard two-level problem (*10*), the magnitude of this matrix element is not critical, since the amplitude of the driving electric field can be adjusted to compensate. The null results for the $E_2 \leftrightarrow E_1$ case for these three symmetric tops with diverse properties provided the initial motivation for the current work.

In an attempt (*5*) to obtain a definitive answer on the observability of the $E_2 \leftrightarrow E_1$ anticrossings, a particularly careful search was carried out, averaging a large number of scans; the search was unsuccessful. Because Zeeman studies had shown that the assignment with $\Delta m_J = 0$ was correct for rows 7 and 8, it was assumed at the time that this was also the case for row 9. It was routine at that time to apply a magnetic field during the search to avoid difficulties in the coupling scheme (see above). If a magnetic field was indeed present, the stronger signal, due to assignment 9a, would have been shifted outside the search region, and only the weaker one, due to assignment 9, would have been present. This is only 0.5% of the stronger line in row 7 and would not have been detected. Unfortunately, the original records do not state explicitly that

the magnetic field was applied. If it was not, then the stronger signal due to row 9a would have been present. This has 3% of the intensity of the line in row 7 and should have been detected under our careful search conditions.

A set of measurements for $J = 2$ in CH_3SiF_3 similar to those discussed above for $J = 1$ in CH_3SiH_3 are shown in Fig. 1 of Ref. (*6*). These measurements correspond to the matrix elements in rows 10–12 in Table XIV. (It should be noted that there is a misprint in Table 2 of Ref. (*6*). In the assignment for the first barrier anticrossing of type $E_3 \leftrightarrow E_2$ listed there ($J = 2$), σ_β should be ∓ 1 rather than ± 1.) It can be seen that the theoretical relative intensity picture and experimental observations for the $J = 2$ barrier anticrossings in CH_3SiF_3 remain largely unchanged from those for $J = 1$ in CH_3SiH_3.

D. New Measurements

With the methods and insight developed in carrying out the analysis described above, it proved possible to observe the missing $E_2 \leftrightarrow E_1$ anticrossing in CH_3SiH_3 discussed in Section 4C. Unfortunately, an external magnetic field could not be applied, and the measurements were made in the ambient field. As a result, three assignments had to be considered, corresponding to row 9, row 9a, and the hybrid of the two. The spin–spin matrix elements of row 9a are noticeably larger than those of row 9, so the assignment was made to row 9a. The spin–rotation interaction could in principle contribute enough to row 9 to make that assignment more favorable, however, so that in spite of the success of the experiment, this assignment ambiguity must be kept in mind.

The experiment was carried out with equipment and techniques very similar to those described earlier (*1–8*). The Pyrex C-field (*4*) was 3.2 cm long. It was used in the configuration which can drive only transitions that conserve the Z-component of the total angular momentum. The spectrum was measured in a static electric field of 536.6 V/cm, which is 0.41 V/cm below the crossing field (precisely calculable from other measurements). The signal is illustrated in Fig. 3. The trace shown was obtained by averaging 16 scans; each scan took 50 sec and the time constant was 1 sec. The observed full-width at half maximum is 30 kHz, as compared to the expected time-of-flight linewidth of 14 kHz. We ascribe this difference to inhomogeneities in the static electric field. (The C-field had been shortened to 3.2 cm to reduce the effects of the field inhomogeneities on the intensity. These effects are very difficult to model and have not been taken into account.)

In order to detect the signal in Fig. 3, the first-order Bessel function J_1 in Eq. (21) of Ref. (*15*) was maximized by setting its argument equal to 1.8. The known tuning rate of the line, $\Delta\mu_{KM} = 370$ kHz/(V/cm), and the known radio frequency, $\nu = 150$ kHz, were then used to obtain an optimum value of $E = 0.7$ V/cm for the RF field to be applied for the previously unobserved very weak $E_2 \leftrightarrow E_1$ spectrum. The observed intensity ratio for the $E_2 \leftrightarrow E_1$ (row 9a of Table XIV) and $E_3 \leftrightarrow E_1$ (row 7) anticrossing lines was 0.040. This is in reasonably good agreement with the ratio of 0.028 calculated for the 3.2-cm-long C-field.

5. SUMMARY

The original goal of this work was to show group-theoretically that certain missing avoided crossing signals mentioned in the previous section were forbidden by symmetry

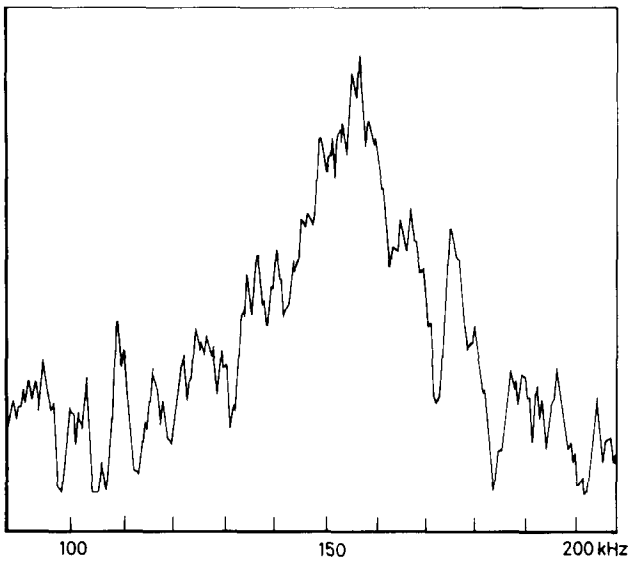

FIG. 3. The $E_2 \leftrightarrow E_1$ avoided-crossing spectrum observed in a static electric field 0.41 V/cm below the crossing field. The line is assigned to the barrier anticrossing ($J = 1$, $K = \pm 1$, $\sigma = \pm 1$, $m_J = \pm 1 \leftrightarrow J = 1$, $K = \pm 1$, $\sigma = 0$, $m_J = \mp 1$), i.e., to row 9a in Table XIV. This represents a class of avoided crossings with very small mixing matrix elements. The successful observation depended critically on an understanding of the AC Stark shift and its effect on the lineshape function.

arguments. When all of our attempts to construct such a group-theoretical proof failed, the goal of the work changed to an attempt to understand why the sensitivity of the molecular-beam electric-resonance method might be greatly reduced for avoided crossing signals of the type under discussion. Once an explanation for this reduction in sensitivity was found (*15*), the group-theoretical analysis developed here was applied to the calculation of the spin–spin mixing matrix elements. These were then used in conjunction with the transition probability for the generalized two-level problem (*15*) to explain at least qualitatively the anomalies observed in the earlier selection rule studies. Finally, the results of Ref. (*15*) were applied to determine the optimum amplitude of the RF electric field in these avoided crossing experiments and, indeed, an example of a missing signal has now been found.

The formalism presented here for dealing with hyperfine Hamiltonians in symmetric-top internal-rotor molecules should be useful in quantitative studies of hyperfine structure in such molecules.

RECEIVED: September 28, 1990

REFERENCES

1. I. OZIER AND W. L. MEERTS, *Phys. Rev. Lett.* **40**, 226–229 (1978).
2. W. L. MEERTS AND I. OZIER, *Phys. Rev. Lett.* **41**, 1109–1112 (1978).
3. I. OZIER AND W. L. MEERTS, *Canad. J. Phys.* **59**, 150–171 (1981).
4. W. L. MEERTS AND I. OZIER, *J. Chem. Phys.* **75**, 596–603 (1981).
5. W. L. MEERTS AND I. OZIER, *J. Mol. Spectrosc.* **94**, 38–54 (1982).

6. W. L. MEERTS AND I. OZIER, *Chem. Phys.* **71,** 401–415 (1982).
7. I. OZIER AND W. L. MEERTS, *Canad. J. Phys.* **62,** 1844–1854 (1984).
8. I. OZIER AND W. L. MEERTS, *Canad. J. Phys.* **63,** 1375 (1985).
9. J. K. G. WATSON, *J. Mol. Spectrosc.* **40,** 536–544 (1971).
10. N. F. RAMSEY, "Molecular Beams," Oxford Univ. Press, London, 1956.
11. P. R. BUNKER "Molecular Symmetry and Spectroscopy," Academic Press, New York, 1979.
12. J. T. HOUGEN AND B. M. DEKOVEN, *J. Mol. Spectrosc.* **98,** 375–391 (1983).
13. M. WONG, I. OZIER, AND W. L. MEERTS, *J. Mol. Spectrosc.* **102,** 89–111 (1983).
14. N. MOAZZEN-AHMADI, I. OZIER, AND W. L. MEERTS, *J. Mol. Spectrosc.* **137,** 166–203 (1989).
15. W. L. MEERTS, I. OZIER, AND J. T. HOUGEN, *J. Chem. Phys.* **90,** 4681–4688 (1989).
16. C. C. LIN AND J. D. SWALEN, *Rev. Mod. Phys.* **31,** 841–892 (1959).
17. H. C. LONGUET-HIGGINS, *Mol. Phys.* **6,** 445–460 (1963).
18. J. T. HOUGEN, *Canad. J. Phys.* **44,** 1169–1182 (1966).
19. P. R. BUNKER, *Mol. Phys.* **9,** 257–264 (1965).
20. A. A. FROST AND B. MUSULIN, *J. Chem. Phys.* **21,** 572–573 (1953).
21. I. M. MILLS, *Mol. Phys.* **7,** 549–563 (1964).
22. W. G. HARTER AND C. W. PATTERSON, *J. Chem. Phys.* **66,** 4872–4885 (1977).
23. E. U. CONDON AND G. H. SHORTLEY, "The Theory of Atomic Spectra," Cambridge Univ. Press, London/New York, 1964.
24. K. VAN HELVOORT, R. FANTONI, W. L. MEERTS, AND J. REUSS, *Chem. Phys. Lett.* **128,** 494–500 (1986).
25. J. T. HOUGEN, *J. Mol. Spectrosc.* **81,** 73–92 (1980).
26. J. H. VAN VLECK, *Rev. Mod. Phys.* **23,** 213–227 (1951).
27. P. B. DAVIES, R. M. NEUMANN, S. C. WOFSY, AND W. KLEMPERER, *J. Chem. Phys.* **55,** 3564–3568 (1971).
28. G. R. GUNTHER-MOHR, C. H. TOWNES, AND J. H. VAN VLECK, *Phys. Rev.* **94,** 1191–1203 (1954).
29. A. R. EDMONDS, "Angular Momentum in Quantum Mechanics," Princeton Univ. Press, Princeton, NJ, 1960 (third printing with corrections, 1974).
30. I. C. BOWATER, J. M. BROWN, AND A. CARRINGTON, *Proc. R. Soc. London Ser. A* **333,** 265–288 (1973).
31. Y. ENDO, C. YAMADA, S. SAITO, AND E. HIROTA, *J. Chem. Phys.* **77,** 3376–3382 (1982).
32. Y. ENDO, S. SAITO, AND E. HIROTA, *J. Chem. Phys.* **81,** 122–135 (1984).
33. J. T. HOUGEN, *J. Chem. Phys.* **57,** 4207–4217 (1972).
34. J. R. DURIG, Y. S. LI, AND C. C. TONG, *J. Mol. Struct.* **14,** 255–260 (1972).